Journal of Mathematical Modeling
Vol. -, No. -, 2026, pp. -. Research Article

JMM

A boundary element method for fractional diffusion-reaction equations

Leila Hasani, AllahBakhsh Yazdani Cherati*, Afshin Babaei

Department of Applied Mathematics, Faculty of Mathematical Sciences, University of Mazandaran, Babolsar, Iran

Email(s): leilahasani92@gmail.com, yazdani@umz.ac.ir, babaei@umz.ac.ir

Abstract. In this study, a boundary element method based on the Caputo derivative is developed for solving the time-fractional diffusion–reaction equation. The model describes anomalous transport behavior coupled with a linear reaction term. The numerical algorithm is implemented in MATLAB, providing an efficient computational framework for fractional analysis. Numerical results for a two-dimensional strip domain show very good agreement with the analytical solution, with a maximum relative error below 0.2%. The method demonstrates stable and accurate behavior for reaction parameters in the range $0 \leq \lambda \lesssim 0.1$, where both boundary and interior errors remain small. For larger reaction parameters, the internal numerical errors increase due to the stronger stiffness introduced by the reaction term. The observed temporal convergence is consistent with the expected behavior of fractional diffusion equations on uniform time grids.

Keywords: Fractional diffusion, Caputo derivative, boundary element method, diffusion-reaction
AMS Subject Classification 2010: 65N38, 35R11, 92B05

1 Introduction

Fractional differential equations (FDEs) have proven highly effective in modeling complex processes with memory and hereditary effects in physics, engineering and biological systems [27, 37, 42, 54]. Among various definitions of fractional derivatives, the Caputo derivative is widely adopted due to its compatibility with standard initial and boundary conditions [21]. In recent years, substantial progress has also been made in the numerical analysis of fractional and nonlocal partial differential equations. This includes stability, convergence, graded-mesh discretizations, and spectral approximations for problems with weakly singular kernels and initial-time singularities [45, 49].

*Corresponding author
Received: 27 December 2025/ Revised: 18 August 2026/ Accepted: 21 August 2026
DOI: 10.22124/jmm.2026.32630.2966

The Boundary Element Method (BEM) is a particularly appealing numerical approach for solving fractional diffusion problems. Specifically, it reduces problem dimensionality and requires only boundary discretization. In the seminal work in [7], a Caputo-based domain BEM (CD-BEM) formulation for time-fractional diffusion equations was developed and validated against several analytical examples. The study demonstrated high accuracy and computational efficiency in handling fractional diffusion governed by the Caputo derivative. At the same time, alternative finite difference, spectral and, adaptive-mesh methods have shown strong performance for related fractional and integro-parabolic models [11, 45, 47, 49]. This provides a broader numerical context for the present BEM-based development.

However, the above formulation focused solely on pure diffusion processes. Alternatively, in real-world settings reaction terms play a crucial role. diffusion-reaction systems arise in a broad range of modeling settings and reaction terms are commonly used to represent growth, decay, or transformation mechanisms [38, 47, 50]. Incorporating a reaction term λu into the fractional diffusion equation enables one to describe growth, decay, or transformation phenomena within a unified nonlocal framework.

In the present work, we extend the original CD-BEM by introducing a constant-coefficient reaction term into a one-dimensional time-fractional diffusion equation, yielding an extended CD-BEM formulation. Analytical solutions for a strip domain under Dirichlet boundary conditions are derived using the Mittag-Leffler function. Numerical simulations are then performed to validate the analytical results. They also assess the influence of the fractional order α and reaction coefficient λ on solution profiles, relative errors, and observed convergence behavior. The present study focuses on the linear constant-coefficient case. This serves as a foundation for future extensions to nonlinear and variable-coefficient problems. It also extends the CD-BEM framework computationally to a reaction-augmented setting and examines its practical behavior across representative parameter ranges. This is also relevant in view of recent studies on fractional evolution equations, adaptive schemes and nonlocal integro-parabolic models [47, 49, 50].

The structure of the paper is organized as follows. In Section 2, a brief review of the related literature and theoretical background is presented. Section 3 introduces the governing time-fractional diffusion-reaction equation and its mathematical formulation. Analytical solutions based on the Mittag-Leffler function are derived in Section 4. Section 5 is devoted to the implementation of the BEM for the extended fractional model. Section 6 presents the numerical results for two illustrative examples, together with a discussion of the numerical error behavior, convergence trends, and the influence of the reaction coefficient. Finally, Section 7 provides concluding remarks and future perspectives of the work.

2 Literature review

The study of diffusion-reaction equations dates back to the pioneering work of Turing (1952), who introduced such models to explain pattern formation in spatially distributed systems [56]. Since then, classical diffusion-reaction systems have become fundamental in describing pattern formation, chemical reactions, and ecological dynamics [39]. Analytical approaches based on separation of variables and Fourier series were widely employed for simple geometries. Green's function methods and eigenfunction expansions subsequently extended their applicability to more general problems.

With the emergence of anomalous diffusion phenomena in complex media, the incorporation of fractional calculus into diffusion-reaction equations gained significant attention [36, 42]. Fractional diffusion-reaction models were developed to capture memory and nonlocal transport effects. Foun-

dational contributions of Seki et al. [52] and Henry et al. [23] established the connection between continuous-time random walks (CTRW) and fractional partial differential operators.

Analytical solutions expressed in terms of Mittag-Leffler and Fox H-functions provided valuable theoretical insights [51], while numerical methods such as finite difference, finite element, and spectral schemes enabled simulations in higher dimensions [60, 61]. Recent advances have further addressed the numerical challenges of fractional evolution equations. These include graded-mesh discretizations, adaptive procedures, and higher-order approximations that resolve initial-time singularities and weakly singular memory kernels [45, 49]. Specifically, we established existence, uniqueness, and sharp error estimates for fractional integro-parabolic equations on adaptive meshes in [49]. In parallel, stability and convergence for spectral approximations of nonlocal weakly singular integro-PDEs were investigated in [45].

Despite these advances, accurate numerical treatment of diffusion-reaction systems with memory effects remains challenging, particularly in the presence of complex boundary conditions, delayed dynamics, and anisotropic transport. Recent studies have highlighted the importance of flexible computational frameworks for such problems, including adaptive moving meshes for singularly perturbed diffusion-reaction equations with Robin or mixed boundary conditions [11, 47]. These developments motivated the use of the BEM and its modern extensions for fractional-order diffusion-reaction models.

The application of the BEM to fractional-order differential equations has attracted significant attention in recent years [4, 8, 9, 12, 27], particularly for handling nonlocal effects and reducing the dimensionality of the computational domain. The seminal work in [7] introduced a formulation based on CD-BEM for anomalous diffusion, demonstrating unconditional stability and computational efficiency even for very small fractional orders ($\alpha = 0.05$). This methodological advance overcame key limitations of earlier Riemann-Liouville-based approaches, which failed for $\alpha < 0.5$. It also consolidated the Laplace domain transform as a powerful strategy for handling fractional time operators. This was achieved without imposing restrictive time-step constraints [1, 7, 10].

Parallel advances in the *Dual-Reciprocity BEM* (DRBEM) have enabled the efficient treatment of inhomogeneous terms, which is crucial for incorporating reaction kinetics into diffusion models. Mohamed in [15] successfully applied DRBEM to fractional biothermomechanics problems, and comparative studies demonstrated a reduction in memory requirements compared to classical BEM [1]. These developments provide the computational framework needed to extend BEM to diffusion-reaction systems.

The theoretical foundation has been strengthened through rigorous stability analyses in fractional Sobolev spaces [26] and the derivation of closed-form Green's functions for fractional boundary value problems [13]. In particular, the work in [20] established the mathematical groundwork for singular kernels which are essential for modeling anomalous transport in nonlocal systems.

Despite this methodological maturity, direct applications of BEM to fractional diffusion-reaction systems are still developing. Recent studies have explored parameter estimation in anomalous diffusion using physics-informed neural networks [55], while non-classical boundary conditions have been shown to play an important role in accurate modeling of diffusion processes [20]. In parallel, fractional PDEs have been widely employed in pharmacokinetics [14, 16, 17, 57–59] and population dynamics [38, 53]. Conversely, the potential of BEM in addressing these challenges remains an active area of research.

Emerging trends suggest that hybrid *Fractional Physics-Informed Neural Network-Boundary Element Method* (FPINN-BEM) frameworks [3, 33] and advanced numerical schemes will shape the field's future trajectory. The development of open-source BEM toolkits [44] and community efforts to establish

benchmarking standards [24, 32] are key enablers for closing the current gap between methodological capability and practical application.

Previous applications of fractional BEM to anomalous thermal transport [34] and heterogeneous media modeling [25] demonstrate the method's capacity for handling complex geometries. Consequently, these mathematical developments provide a viable framework for extending CD-BEM to diffusion-reaction formulations.

3 Mathematical model

In a general framework, time-fractional diffusion-reaction equations in two spatial dimensions with anisotropic diffusion are given by

$$\frac{\partial^\alpha u(x,y,t)}{\partial t^\alpha} = D_x \frac{\partial^2 u(x,y,t)}{\partial x^2} + D_y \frac{\partial^2 u(x,y,t)}{\partial y^2} + R(u(x,y,t)), \quad (x,y) \in \Omega \subset \mathbb{R}^2,\ t > 0, \tag{1}$$

where $u(x,y,t)$ denotes the state variable (e.g., concentration, temperature), $0 < \alpha \leq 1$ is the order of the Caputo fractional time derivative, $D_x > 0$ and $D_y > 0$ are the diffusion coefficients in the x- and y-directions, and $R(u)$ denotes the reaction term. Equation (1) is introduced only to indicate the broader class of models to which the present problem belongs. In the current work, the analysis and numerical treatment are restricted to the linear constant-coefficient case

$$R(u) = -\lambda u, \tag{2}$$

where $\lambda \geq 0$ is the decay rate. In this setting, the governing model reduces to

$$\frac{\partial^\alpha u(x,y,t)}{\partial t^\alpha} = D_x \frac{\partial^2 u(x,y,t)}{\partial x^2} + D_y \frac{\partial^2 u(x,y,t)}{\partial y^2} - \lambda u(x,y,t), \quad (x,y) \in \Omega,\ t > 0. \tag{3}$$

From a physical perspective, the reaction term $-\lambda u$ represents a linear sink or a first-order decay process, which is characteristic of systems where the quantity u is consumed, dissipated, or absorbed at a rate proportional to its local value. This formulation is widely applicable in mass transport and thermal dissipation models, ensuring that the governing equation remains both mathematically tractable and physically consistent.

The purpose of the present work is to analyze this special case and validate its solutions through analytical and numerical methods (in particular, the BEM). The novelty of the present work does not lie in developing a new continuous existence theory for the general nonlinear problem (1). Rather, it lies in formulating and assessing a BEM treatment for the linear time-fractional diffusion-reaction problem (3).

3.1 Assumptions, well-posed setting, and data compatibility

Throughout this paper, we consider the continuous problem for the linear model (3). We assume that the boundary $\partial\Omega$ is sufficiently smooth, or piecewise smooth in the standard sense required by the boundary integral formulation. The initial data u_0, the Dirichlet boundary data f, and the Neumann boundary data g are assumed to be sufficiently regular. Under this assumption, the Caputo derivative, boundary traces, and normal derivatives are well defined, and the integral formulation used later is meaningful. In

addition, for each fixed time t, the solution is assumed to be sufficiently smooth in the spatial variables, for instance $u(\cdot,t) \in C^2(\Omega)$, so that the second-order spatial derivatives appearing in Equation (3) are well defined. In particular, the temporal regularity is assumed to be adequate for the Caputo derivative of order $0 < \alpha < 1$, for example in the standard sense that u is absolutely continuous with respect to t on $[0,T]$ for each fixed spatial point.

Under such assumptions, the linear time-fractional diffusion-reaction Equation (3) is considered in the usual well-posed framework adopted in the literature on fractional and integro-parabolic equations. Related analyses addressing existence, uniqueness, stability, and convergence under appropriate regularity hypotheses may be found, for example, in [45, 47, 49]. The present work therefore does not claim a new well-posedness result for the continuous problem; rather, it develops the corresponding boundary element formulation for this class of models.

When Dirichlet boundary data are prescribed (see subsection below), the standard compatibility condition at the initial time is assumed on Γ_D, namely

$$u_0(x,y) = f(x,y,0), \qquad (x,y) \in \Gamma_D. \tag{4}$$

If mixed boundary conditions are imposed, the data are further assumed to be mutually compatible in the standard trace sense. This is particularly important in fractional diffusion problems, where solutions may exhibit reduced regularity near $t = 0$, and such behavior influences the stability and convergence of numerical approximations [47, 49].

3.2 Initial and boundary conditions

The system is governed by mixed boundary conditions, namely the Dirichlet condition

$$u(x,y,t) = f(x,y,t), \quad (x,y) \in \Gamma_D, \tag{5}$$

and the Neumann condition

$$q(x,y,t) = \frac{\partial u(x,y,t)}{\partial n} = g(x,y,t), \quad (x,y) \in \Gamma_N, \tag{6}$$

where $\Gamma_D \subset \partial\Omega$ is the Dirichlet boundary on which the solution values are prescribed, $\Gamma_N \subset \partial\Omega$ is the Neumann boundary on which the normal derivative values are imposed, and q denotes the normal flux. The normal derivative is given by $\frac{\partial u}{\partial n} = \nabla u \cdot \mathbf{n}$ where $\mathbf{n}$ denotes the unit outward normal vector to the boundary. The boundary is decomposed as $\partial\Omega = \Gamma_D \cup \Gamma_N$ in the trace sense, and the Dirichlet and Neumann parts may meet only at finitely many corner points. This convention is adopted to avoid the ambiguity associated with a strict pointwise interpretation of disjointness on piecewise smooth boundaries.

We complete the formulation with the initial condition

$$u(x,y,0) = u_0(x,y), \quad (x,y) \in \Omega, \tag{7}$$

where $u_0(x,y)$ denotes the initial distribution of the field quantity over the domain Ω.

3.3 Special cases

The general model encompasses several well-known equations as special cases. When $\alpha = 1$, the temporal derivative reduces to its classical form, and the governing equation becomes the standard diffusion-reaction equation

$$\frac{\partial u}{\partial t} = D_x \frac{\partial^2 u}{\partial x^2} + D_y \frac{\partial^2 u}{\partial y^2} - \lambda u. \tag{8}$$

In the absence of a reaction term, i.e., when $\lambda = 0$, the model simplifies to the time-fractional diffusion equation

$$\frac{\partial^\alpha u}{\partial t^\alpha} = D_x \frac{\partial^2 u}{\partial x^2} + D_y \frac{\partial^2 u}{\partial y^2}. \tag{9}$$

Furthermore, if the diffusion process is isotropic with $D_x = D_y = D$, the governing equation reduces to

$$\frac{\partial^\alpha u}{\partial t^\alpha} = D\nabla^2 u - \lambda u. \tag{10}$$

These reductions highlight the versatility of the fractional anisotropic diffusion-reaction model in capturing various diffusion and dissipation regimes. The anisotropic case $D_x \neq D_y$ is particularly relevant in applications where transport properties differ by direction, including heterogeneous and structured media [5, 20, 23, 58, 59]. Furthermore, the isotropic and one-dimensional limits discussed above provide connections to well-established classical and fractional models in the literature.

3.4 Caputo fractional derivative

For completeness, the Caputo fractional derivative of order α, with $0 < \alpha < 1$, is defined by

$${}^C D_t^\alpha u(t) = \frac{1}{\Gamma(1-\alpha)} \int_0^t (t-\tau)^{-\alpha} \frac{\partial u(\tau)}{\partial \tau} \, d\tau, \tag{11}$$

where $\Gamma(\cdot)$ denotes the Gamma function. This operator incorporates memory effects and is widely used in the modeling of anomalous diffusion processes. Its validity requires suitable temporal regularity of the solution, as noted above, and it is precisely this nonlocal time dependence that distinguishes the present model from its classical counterpart.

3.5 Remark on regularity near the initial time

Even for smooth input data, solutions of time-fractional diffusion-type equations may exhibit weak singular behavior near $t = 0$. This reduced regularity is well documented in the literature and plays an important role in the stability and convergence analysis of numerical schemes. It often motivates the use of graded or adaptive temporal meshes [45, 47, 49]. In the present work, we develop the BEM formulation under the regularity and compatibility assumptions stated above and use numerical experiments to examine the corresponding solution behavior for different values of α and λ.

4 Analytical solution in rectangular and square domains

In the present study, analytical results are proved only for rectangular and square domains. These closed-form expressions are used as benchmark solutions for validating the proposed numerical treatment in geometries where the corresponding sine-eigenfunction structure is available. Such analytical benchmark solutions are particularly useful for assessing numerical schemes for time-fractional diffusion-reaction models, especially in view of the reduced temporal regularity that may arise near the initial time [47,49]. For the validity of the analytical derivation, we assume that the solution $u(x,y,t)$ is sufficiently smooth so that the Caputo derivative and the boundary traces are well-defined. In addition, we assume that the initial and boundary data satisfy the necessary compatibility conditions at $t = 0$ [45].

We consider the two-dimensional domain $\Omega = [0,L_x] \times [0,L_y]$ with generally anisotropic diffusion coefficients D_x and D_y, in which the dynamics are governed by

$$\frac{\partial^\alpha u}{\partial t^\alpha} = D_x \frac{\partial^2 u}{\partial x^2} + D_y \frac{\partial^2 u}{\partial y^2} - \lambda\, u, \quad 0 < \alpha \leq 1, \tag{12}$$

subject to the Dirichlet boundary conditions

$$u(0,y,t) = U_0, \quad u(L_x,y,t) = 0, \tag{13}$$

$$u(x,0,t) = U_0, \quad u(x,L_y,t) = 0, \tag{14}$$

and the separable initial condition

$$u(x,y,0) = U_0 \left(1 - \frac{x}{L_x}\right)\left(1 - \frac{y}{L_y}\right). \tag{15}$$

It is worth noting that the initial condition (15) is constructed to be strictly compatible with the boundary values (13–14) at $t = 0$, ensuring the existence of a stable solution in the trace sense.

A standard boundary-lifting transformation converts the nonhomogeneous Dirichlet conditions into homogeneous ones. The solution is then sought by separation of variables for the transformed problem in the form $u(x,y,t) = \phi(x)\psi(y)T(t)$. Specifically, the prescribed boundary values are first represented by an auxiliary profile consistent with (13–15), after which the remaining unknown satisfies homogeneous conditions. The spatial eigenvalue problems are obtained as

$$\phi''(x) + \nu_m \phi(x) = 0, \quad \nu_m = \left(\frac{m\pi}{L_x}\right)^2, \quad m = 1,2,\ldots, \tag{16}$$

$$\psi''(y) + \eta_n \psi(y) = 0, \quad \eta_n = \left(\frac{n\pi}{L_y}\right)^2, \quad n = 1,2,\ldots, \tag{17}$$

with eigenfunctions

$$\phi_m(x) = \sin\left(\frac{m\pi x}{L_x}\right), \quad \psi_n(y) = \sin\left(\frac{n\pi y}{L_y}\right). \tag{18}$$

The combined separation constant is

$$\mu_{mn} = D_x\, \nu_m + D_y\, \eta_n = D_x \left(\frac{m\pi}{L_x}\right)^2 + D_y \left(\frac{n\pi}{L_y}\right)^2, \tag{19}$$

where μ_{mn} represents the combined spatial separation constants arising from the anisotropic diffusion coefficients D_x and D_y, determining the effective diffusion rate in each eigenmode of the rectangular domain [23, 52].

The temporal modes $T_{mn}(t)$ denote the modal fractional relaxation functions associated with the Caputo derivative, satisfying

$$ {}^{C}D_t^{\alpha} T_{mn}(t) = -(\mu_{mn} + \lambda)\, T_{mn}(t), \tag{20} $$

whose closed-form representation in terms of the Mittag-Leffler function is standard for linear time-fractional models [23, 42]:

$$ T_{mn}(t) = E_{\alpha}(-[\mu_{mn} + \lambda] t^{\alpha}), \tag{21} $$

where $E_{\alpha}(z)$ denotes the one-parameter Mittag-Leffler function defined as

$$ E_{\alpha}(z) = \sum_{k=0}^{\infty} \frac{z^k}{\Gamma(\alpha k + 1)}. \tag{22} $$

Here, $T_{mn}(t)$ represents the temporal modes governed by the fractional Caputo derivative and expressed via the Mittag-Leffler function, describing the memory-dependent relaxation of each spatial mode [23, 42].

Applying the orthogonality of sine functions to match the initial condition (15) yields

$$ C_{mn} = \frac{4U_0}{mn\pi^2}, \tag{23} $$

where C_{mn} are the expansion coefficients obtained from the orthogonality of sine eigenfunctions used to match the separable initial profile [38, 42].

Substituting (18), (19), (21) and (23) into the general separated form provides the complete anisotropic rectangular solution:

$$ \begin{aligned} u(x,y,t) = U_0 &\left(1 - \frac{x}{L_x}\right)\left(1 - \frac{y}{L_y}\right) \\ &- \frac{4U_0}{\pi^2} \sum_{m=1}^{\infty} \sum_{n=1}^{\infty} \frac{\sin\left(\frac{m\pi x}{L_x}\right) \sin\left(\frac{n\pi y}{L_y}\right)}{mn} \\ &\times E_{\alpha}\left(-\left[D_x \left(\frac{m\pi}{L_x}\right)^2 + D_y \left(\frac{n\pi}{L_y}\right)^2 + \lambda\right] t^{\alpha}\right). \end{aligned} \tag{24} $$

In the special case of a square anisotropic domain $L_x = L_y = L$, the eigenvalues in (16) and (17) reduce to $(m\pi/L)^2$ and $(n\pi/L)^2$ respectively, leading to $\mu_{mn} = D_x(m\pi/L)^2 + D_y(n\pi/L)^2$ in (19), while the solution (24) remains valid with these substitutions.

For an isotropic rectangular domain, setting $D_x = D_y = D$ gives

$$ \mu_{mn} = D\left[\left(\frac{m\pi}{L_x}\right)^2 + \left(\frac{n\pi}{L_y}\right)^2\right], \tag{25} $$

while in the isotropic square case ($L_x = L_y = L$, $D_x = D_y = D$) one finds

$$ \mu_{mn} = D\left[\left(\frac{m\pi}{L}\right)^2 + \left(\frac{n\pi}{L}\right)^2\right]. \tag{26} $$

Finally, consider the one-dimensional domain $\Omega = [0, L_x]$ with $D_x = D$ and Dirichlet boundaries $u(0,t) = U_0$ and $u(L_x,t) = 0$. In this case, the solution reduces to

$$u(x,t) = U_0\left(1 - \frac{x}{L_x}\right) - \frac{2U_0}{\pi}\sum_{m=1}^{\infty}\frac{\sin\left(\frac{m\pi x}{L_x}\right)}{m}E_\alpha\left(-\left[D\left(\frac{m\pi}{L_x}\right)^2 + \lambda\right]t^\alpha\right). \tag{27}$$

5 Formulation and implementation of BEM

5.1 Boundary integral equation formulation

According to the BEM, the formulation can be derived using the method of weighted residuals. Let $\Omega \subset \mathbb{R}^2$ be a bounded domain with boundary $\partial\Omega$. We assume that for each fixed time t, the solution satisfies

$$u(\cdot,t) \in H^1(\Omega), \tag{28}$$

and the weight (test) function $w(\xi, X)$ belongs to the same admissible space. Multiplying the governing equation by the test function and integrating over the spatial domain Ω yields the weak (variational) formulation of the problem.

We write the residual of the governing equation as follows [6]

$$R(X,t) = \frac{\partial^\alpha u}{\partial t^\alpha} - D_x\frac{\partial^2 u}{\partial x^2} - D_y\frac{\partial^2 u}{\partial y^2} + \lambda u, \tag{29}$$

Applying the method of weighted residuals, we obtain

$$\int_\Omega\left(\frac{\partial^\alpha u}{\partial t^\alpha} - D_x\frac{\partial^2 u}{\partial x^2} - D_y\frac{\partial^2 u}{\partial y^2} + \lambda u\right)w(\xi,X)\,d\Omega(X) = 0, \tag{30}$$

which represents the weak formulation of the governing fractional diffusion-reaction equation.

For convenience, the above integral is decomposed into three components:

1. Laplacian terms

$$\int_\Omega\left(-D_x\frac{\partial^2 u}{\partial x^2} - D_y\frac{\partial^2 u}{\partial y^2}\right)w(\xi,X)\,d\Omega(X), \tag{31}$$

2. Caputo derivative term

$$\int_\Omega\frac{\partial^\alpha u}{\partial t^\alpha}\,w(\xi,X)\,d\Omega(X), \tag{32}$$

3. Reaction term

$$\int_\Omega \lambda u\,w(\xi,X)\,d\Omega(X), \tag{33}$$

where $w(\xi,X)$ denotes the weight function used to project the residual $R(X,t)$ onto the approximation space such that the inner product of the residual with the test function vanishes. Here, $X \in \Omega$ denotes the integration variable over the spatial domain, while ξ represents the source (collocation) point located either inside the domain or on its boundary.

5.2 Laplacian integrals

Similar to the approach presented in [7], the fundamental solution $\bar{w}(\xi,X)$ for the anisotropic steady-state equation is chosen, where ξ is the source point and X is the field point. The fundamental solution satisfies

$$D_x\frac{\partial^2\bar{w}}{\partial x^2}+D_y\frac{\partial^2\bar{w}}{\partial y^2}=-\delta(\xi,X). \tag{34}$$

Here, $\delta(\xi,X)$ is the Dirac delta function, representing a unit point source located at ξ. It satisfies

$$\int_\Omega \delta(\xi,X)\,dX=1, \qquad \delta(\xi,X)=0 \quad \text{for } X\neq\xi, \qquad \int_\Omega f(X)\,\delta(\xi,X)\,dX=f(\xi), \tag{35}$$

for any sufficiently smooth function $f(X)$, provided that $\xi\in\Omega$.

The fundamental solution is obtained by introducing the scaled coordinates

$$\eta=x-\xi_x, \qquad \zeta=\sqrt{\frac{D_x}{D_y}}\,(y-\xi_y). \tag{36}$$

Accordingly, the anisotropic diffusion operator is transformed into a scaled standard two-dimensional Laplacian

$$D_x\frac{\partial^2}{\partial x^2}+D_y\frac{\partial^2}{\partial y^2}=D_x\left(\frac{\partial^2}{\partial\eta^2}+\frac{\partial^2}{\partial\zeta^2}\right). \tag{37}$$

Moreover, the Dirac delta function transforms according to

$$\delta(x-\xi_x)\delta(y-\xi_y)=\sqrt{\frac{D_x}{D_y}}\,\delta(\eta)\delta(\zeta). \tag{38}$$

Therefore, by using the classical logarithmic fundamental solution of the two-dimensional Laplacian and accounting for the Jacobian of the coordinate transformation, the anisotropic problem leads to the following fundamental solution [4]

$$\bar{w}(\xi,X)=\frac{1}{2\pi\sqrt{D_xD_y}}\ln\left(\frac{1}{r}\right), \quad r=\sqrt{(x-\xi_x)^2+\frac{D_x}{D_y}(y-\xi_y)^2}, \tag{39}$$

where r represents the normalized distance between the source point $\xi=(\xi_x,\xi_y)$ and the field point $X=(x,y)$. This fundamental solution satisfies Equation (34).

Here $\mathbf{n}=(n_x,n_y)$ is the unit outward normal vector at the boundary point X, with n_x and n_y denoting its Cartesian components. The normal derivative, denoted by $Q(\xi,X)$, is given by

$$Q(\xi,X)=\frac{\partial\bar{w}}{\partial n}=\frac{\partial\bar{w}}{\partial x}n_x+\frac{\partial\bar{w}}{\partial y}n_y. \tag{40}$$

For the Laplacian part (31), we apply integration by parts. In the present formulation, the weight function $w(\xi,X)$ is chosen as the fundamental solution of the anisotropic steady-state operator

$$w(\xi,X)=\bar{w}(\xi,X). \tag{41}$$

By substituting this choice, the second Green's identity for the anisotropic Laplacian terms yields

$$\int_\Omega \left(D_x \frac{\partial^2 u}{\partial x^2} + D_y \frac{\partial^2 u}{\partial y^2} \right) \bar{w}\, d\Omega = \int_{\partial\Omega} q\bar{w}\, dS - \int_{\partial\Omega} uQ\, dS + \int_\Omega u \left(D_x \frac{\partial^2 \bar{w}}{\partial x^2} + D_y \frac{\partial^2 \bar{w}}{\partial y^2} \right) d\Omega, \tag{42}$$

where S denotes the boundary (or boundary curve in 2D) over which the boundary integrals are evaluated. Since the fundamental solution satisfies Equation (34), and using the sifting property of the Dirac delta function in (35), the domain integral on the right-hand side of Equation (42) simplifies to

$$\int_\Omega u \left(D_x \frac{\partial^2 \bar{w}}{\partial x^2} + D_y \frac{\partial^2 \bar{w}}{\partial y^2} \right) d\Omega = -c(\xi) u(\xi), \tag{43}$$

where $c(\xi)$ is the standard boundary element geometry coefficient, dependent on the position of the source point ξ.

Substituting Equation (43) into the weighted residual formulation given in Equation (30) yields the following boundary integral equation:

$$\begin{aligned} c(\xi) u(\xi,t) = & \int_{\partial\Omega} q(X,t)\, \bar{w}(\xi,X)\, dS(X) - \int_{\partial\Omega} u(X,t)\, Q(\xi,X)\, dS(X) \\ & - \int_\Omega \frac{\partial^\alpha u(X,t)}{\partial t^\alpha}\, \bar{w}(\xi,X)\, d\Omega(X) - \lambda \int_\Omega u(X,t)\, \bar{w}(\xi,X)\, d\Omega(X). \end{aligned} \tag{44}$$

In the anomalous diffusion equation (without the reaction term), the domain integral included only the fractional time derivative $\frac{\partial^\alpha u}{\partial t^\alpha}$. We added the term $\lambda u(X,t)$ to the domain integral to represent the effect of the reaction.

The term $c(\xi)$ in the boundary integral equation is computed using the internal angle at the boundary point ξ. This term plays a critical role in ensuring solution accuracy at geometric discontinuities such as corners and edges. For anisotropic media where the diffusion coefficients D_x and D_y differ, the general expression for $c(\xi)$ is given by [8]

$$c(\xi) = \frac{1}{2\pi} \left[\tan^{-1} \left(\frac{D_x}{D_y} \tan\theta_2 \right) - \tan^{-1} \left(\frac{D_x}{D_y} \tan\theta_1 \right) \right], \tag{45}$$

where θ_1 and θ_2 are the angles between the outward normals of the two adjacent boundary elements and a fixed reference direction (see Figure 1). Note that the expression for $c(\xi)$ given in Equation (45) assumes that the diffusion tensor is diagonal in the chosen coordinate system. In other words, the principal axes of diffusion are aligned with the coordinate axes.

For the special case of isotropic media ($D_x = D_y$), Equation (45) simplifies to the well-known geometric form

$$c(\xi) = \frac{\theta_2 - \theta_1}{2\pi}. \tag{46}$$

The value of $c(\xi)$ is intricately tied to the local geometry of the boundary, reflecting the topological characteristics of the point ξ within the BEM framework. For a smooth boundary point, where the internal angle spanned by the adjacent boundary elements is π (i.e., $\theta_2 - \theta_1 = \pi$), the coefficient $c(\xi)$ adopts a value of $\frac{1}{2}$. At an internal corner, where the angular difference exceeds π ($\theta_2 - \theta_1 > \pi$), $c(\xi)$ surpasses $\frac{1}{2}$, accounting for the increased solid angle subtended by the boundary. Conversely, at an

external corner, where $\theta_2 - \theta_1 < \pi$, $c(\xi)$ falls below $\frac{1}{2}$. Finally, when ξ lies inside the domain, the full angular range of 2π radians ($\theta_2 - \theta_1 = 2\pi$) corresponds to $c(\xi) = 1$. These variations underscore the dependency of $c(\xi)$ on the local boundary topology, a critical factor in ensuring the accuracy and stability of the BEM formulation, particularly in the context of anomalous diffusion problems with fractional-order derivatives.

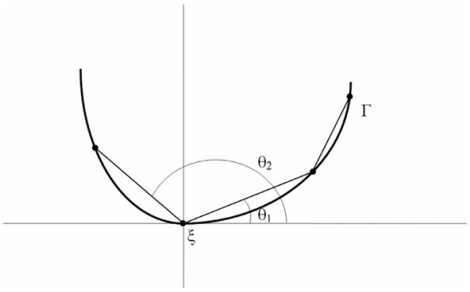

Figure 1: Definition of θ_1 and θ_2 for computing $c(\xi)$ at the corner point $\xi \in \Gamma$

5.3 Temporal discretization

For numerical solution, we discretize time into intervals $[t_n, t_{n+1}]$ with $t_{n+1} = (n+1)\Delta t$, where Δt is the time step size. We assume a linear approximation for $u(X,\tau)$ within a time step [7]

$$u(X,\tau) = \frac{t_{n+1} - \tau}{\Delta t} u_n(X) + \frac{\tau - t_n}{\Delta t} u_{n+1}(X), \tag{47}$$

where $u_n(X) = u(X,t_n)$ and $u_{n+1}(X) = u(X,t_{n+1})$ denote the values of u at the current and next time levels, respectively.

Based on the linear approximation, the time derivative at each discrete time step is expressed as

$$\frac{\partial u}{\partial \tau} \approx \frac{u_{n+1} - u_n}{\Delta t}. \tag{48}$$

The Caputo fractional derivative for $0 < \alpha < 1$, evaluated at a discrete time level t_{n+1}, can be represented as

$$\left.\frac{\partial^\alpha u}{\partial t^\alpha}\right|_{t=t_{n+1}} = \frac{1}{\Gamma(1-\alpha)} \int_0^{t_{n+1}} \frac{1}{(t_{n+1} - \tau)^\alpha} \frac{\partial u(X,\tau)}{\partial \tau} d\tau. \tag{49}$$

To numerically evaluate this integral at time $t_{n+1} = (n+1)\Delta t$, the interval $[0, t_{n+1}]$ is divided into subintervals $[t_k, t_{k+1}]$

$$\left.\frac{\partial^\alpha u}{\partial t^\alpha}\right|_{t=t_{n+1}} = \frac{1}{\Gamma(1-\alpha)} \sum_{k=0}^{n} \int_{t_k}^{t_{k+1}} \frac{1}{(t_{n+1} - \tau)^\alpha} \frac{\partial u(X,\tau)}{\partial \tau} d\tau. \tag{50}$$

According to the finite difference approximation for the time derivative (see Equation (47)), we obtain

$$\left.\frac{\partial^\alpha u}{\partial t^\alpha}\right|_{t=t_{n+1}} \approx \frac{1}{\Gamma(1-\alpha)} \sum_{k=0}^{n} \int_{t_k}^{t_{k+1}} \frac{1}{(t_{n+1} - \tau)^\alpha} \frac{u_{k+1} - u_k}{\Delta t} d\tau$$

$$= \frac{1}{\Gamma(1-\alpha)} \sum_{k=0}^{n} \frac{u_{k+1}-u_k}{\Delta t} \int_{t_k}^{t_{k+1}} \frac{1}{(t_{n+1}-\tau)^{\alpha}} d\tau. \tag{51}$$

By evaluating the integral in Equation (51) using the standard procedure for Caputo derivative discretization [7], the Caputo fractional derivative at t_{n+1} can be expressed as

$$\frac{\partial^{\alpha} u(X,t_{n+1})}{\partial t^{\alpha}} \approx \frac{1}{\Gamma(2-\alpha)\Delta t^{\alpha}} \left[u_{n+1}(X) - u_n(X) + \sum_{k=0}^{n-1} B_{(n+1)(k+1)} (u_{k+1}(X) - u_k(X)) \right], \tag{52}$$

where

$$B_{(n+1)(k+1)} = (n+1-k)^{1-\alpha} - (n-k)^{1-\alpha}. \tag{53}$$

The coefficients $B_{n+1,k+1}$ are history-dependent weights that characterize the memory effect intrinsic to the Caputo fractional derivative. As $(n+1-j)$ increases, these weights decrease, indicating that the influence of earlier time levels diminishes, particularly for smaller values of α. The discretized formula is valid for $n \geq 1$. For $n = 0$, the summation term vanishes and the formula reduces to

$$\left. \frac{\partial^{\alpha} u}{\partial t^{\alpha}} \right|_{t_1} \approx \frac{1}{\Gamma(2-\alpha)\Delta t^{\alpha}} [u_1 - u_0]. \tag{54}$$

By substituting the discretized formula for the Caputo fractional derivative into Equation (44), we obtain

$$\begin{aligned} c(\xi)\, u_{n+1}(\xi) \approx & \int_{\partial\Omega} q_{n+1}(X)\, \bar{w}(\xi,X)\, dS(X) - \int_{\partial\Omega} u_{n+1}(X)\, Q(\xi,X)\, dS(X) \\ & - \frac{1}{\Gamma(2-\alpha)\,\Delta t^{\alpha}} \int_{\Omega} \Big[u_{n+1}(X) - u_n(X) \\ & + \sum_{k=0}^{n-1} B_{(n+1)(k+1)} \left(u_{k+1}(X) - u_k(X) \right) \Big] \bar{w}(\xi,X)\, d\Omega(X) \\ & - \lambda \int_{\Omega} u_{n+1}(X)\, \bar{w}(\xi,X)\, d\Omega(X), \end{aligned} \tag{55}$$

where $\bar{w}(\xi,X)$ denotes the fundamental solution of the Laplace operator and is used consistently as the weighting function for all domain terms.

5.4 Spatial discretization and matrix formulation

As previously discussed, the BEM is a numerical technique for solving partial differential equations, particularly those arising in continuum mechanics and potential problems. In BEM, the main idea is to reformulate the governing differential equations as boundary integral equations by using appropriate fundamental solutions. Thus, the problem is reduced from the domain to its boundary, significantly decreasing computational effort, especially for problems with infinite or semi-infinite domains.

In the present approach, the boundary Γ of the domain Ω is discretized into a finite number of linear elements, and the interior Ω is divided into triangular cells. The variables q (e.g., flux) and u (e.g., potential) are both interpolated using piecewise linear functions at the nodes defined on the boundary and within the domain.

The boundary integrals encountered in the formulation are approximated by summing the contributions over each boundary element

$$\int_{\Gamma} f(\mathbf{x})\, d\Gamma \approx \sum_{e=1}^{N_\Gamma} \int_{\Gamma_e} f(\mathbf{x})\, d\Gamma, \tag{56}$$

where N_Γ denotes the number of boundary elements and Γ_e is an individual boundary element. On each linear element, the function $f(\mathbf{x})$ is interpolated using its nodal values, and the integral over each element is computed via standard quadrature rules, such as the midpoint or Gaussian quadrature.

Similarly, for the domain Ω, the area integrals are decomposed as

$$\int_{\Omega} f(\mathbf{x})\, d\Omega \approx \sum_{c=1}^{N_\Omega} \int_{\Omega_c} f(\mathbf{x})\, d\Omega, \tag{57}$$

where N_Ω is the number of triangular cells and Ω_c denotes each triangular cell. Within each triangle, linear interpolation and suitable numerical integration methods, such as area-coordinate-based quadrature, are used.

Applying such discretization to the time-integral form in Equation (55) transforms the continuum problem into a matrix equation. This equation relates the nodal values of the variables on the boundary and within the domain. The resulting discrete matrix equation takes the following form

$$\mathbf{H}u_{n+1} = \mathbf{G}q_{n+1} - \frac{1}{\Gamma(2-\alpha)\Delta t^{\alpha}}\,\mathbf{M}\left[(u_{n+1}-u_n) + \sum_{k=0}^{n-1} B_{(n+1)(k+1)}\,(u_{k+1}-u_k)\right] - \lambda\,\mathbf{M}u_{n+1}, \tag{58}$$

where all matrices and vectors are constructed from the contributions of the discretized boundary and domain integrals, as described above. Consequently,

$$\begin{aligned}\begin{bmatrix}\mathbf{H}^{bb} & \mathbf{H}^{bd}\\ \mathbf{H}^{db} & \mathbf{H}^{dd}\end{bmatrix}\begin{bmatrix}\mathbf{u}^{b}_{n+1}\\ \mathbf{u}^{d}_{n+1}\end{bmatrix} &= \begin{bmatrix}\mathbf{G}^{bb} & \mathbf{G}^{bd}\\ \mathbf{G}^{db} & \mathbf{G}^{dd}\end{bmatrix}\begin{bmatrix}\mathbf{q}^{b}_{n+1}\end{bmatrix}\\ &\quad - \frac{1}{\Gamma(2-\alpha)\Delta t^{\alpha}}\begin{bmatrix}\mathbf{M}^{bb} & \mathbf{M}^{bd}\\ \mathbf{M}^{db} & \mathbf{M}^{dd}\end{bmatrix}\left(\begin{bmatrix}\mathbf{u}^{b}_{n+1}-\mathbf{u}^{b}_{n}\\ \mathbf{u}^{d}_{n+1}-\mathbf{u}^{d}_{n}\end{bmatrix}\right.\\ &\quad \left. + \sum_{k=0}^{n-1} B_{(n+1)(k+1)}\begin{bmatrix}\mathbf{u}^{b}_{k+1}-\mathbf{u}^{b}_{k}\\ \mathbf{u}^{d}_{k+1}-\mathbf{u}^{d}_{k}\end{bmatrix}\right)\\ &\quad - \lambda\begin{bmatrix}\mathbf{M}^{bb} & \mathbf{M}^{bd}\\ \mathbf{M}^{db} & \mathbf{M}^{dd}\end{bmatrix}\begin{bmatrix}\mathbf{u}^{b}_{n+1}\\ \mathbf{u}^{d}_{n+1}\end{bmatrix}.\end{aligned} \tag{59}$$

Here, $\mathbf{u}^{b}_{n+1}$ and $\mathbf{u}^{d}_{n+1}$ denote the vectors of u values at boundary and domain nodes at time t_{n+1}, respectively, while $\mathbf{q}^{b}_{n+1}$ is the vector of flux q values at the boundary nodes. The superscripts 'b' and 'd' denote indices related to the boundary and domain nodes, respectively, and define the block structure of the system matrices. For instance, $\mathbf{H}^{bb}$ represents the interaction between boundary nodes, whereas $\mathbf{H}^{bd}$ and $\mathbf{H}^{db}$ describe the coupling between boundary and domain nodes. The matrices $\mathbf{G}$ and $\mathbf{H}$ are constructed from the boundary integrals $\int_\Gamma qw\,d\Gamma$ and $\int_\Gamma uQ\,d\Gamma$, respectively, with $\mathbf{H}$ also incorporating the $c(\xi)$ term. The matrix $\mathbf{M}$ is assembled from the domain integral $\int_\Omega uw\,d\Omega$. For internal domain

nodes, $c(\xi) = 1$, which contributes to the identity matrix within the block $\mathbf{H}^{dd}$. To proceed with the solution, all terms involving $u_{n+1}$are collected on one side of the equation

$$\begin{aligned}
&\begin{bmatrix} \mathbf{H}^{bb} + \dfrac{1}{\Gamma(2-\alpha)\Delta t^{\alpha}}\mathbf{M}^{bb} + \lambda\mathbf{M}^{bb} & \dfrac{1}{\Gamma(2-\alpha)\Delta t^{\alpha}}\mathbf{M}^{bd} + \lambda\mathbf{M}^{bd} \\ \mathbf{H}^{db} + \dfrac{1}{\Gamma(2-\alpha)\Delta t^{\alpha}}\mathbf{M}^{db} + \lambda\mathbf{M}^{db} & \mathbf{I} + \dfrac{1}{\Gamma(2-\alpha)\Delta t^{\alpha}}\mathbf{M}^{dd} + \lambda\mathbf{M}^{dd} \end{bmatrix} \begin{bmatrix} \mathbf{u}^{b}_{n+1} \\ \mathbf{u}^{d}_{n+1} \end{bmatrix} \\
&= \begin{bmatrix} \mathbf{G}^{bb} & \mathbf{G}^{bd} \\ \mathbf{G}^{db} & \mathbf{G}^{dd} \end{bmatrix} \begin{bmatrix} \mathbf{q}^{b}_{n+1} \end{bmatrix} + \frac{1}{\Gamma(2-\alpha)\Delta t^{\alpha}} \begin{bmatrix} \mathbf{M}^{bb} & \mathbf{M}^{bd} \\ \mathbf{M}^{db} & \mathbf{M}^{dd} \end{bmatrix} \begin{bmatrix} \mathbf{u}^{b}_{n} \\ \mathbf{u}^{d}_{n} \end{bmatrix} \\
&- \frac{1}{\Gamma(2-\alpha)\Delta t^{\alpha}} \begin{bmatrix} \mathbf{M}^{bb} & \mathbf{M}^{bd} \\ \mathbf{M}^{db} & \mathbf{M}^{dd} \end{bmatrix} \sum_{k=0}^{n-1} B_{(n+1)(k+1)} \begin{bmatrix} \mathbf{u}^{b}_{k+1} - \mathbf{u}^{b}_{k} \\ \mathbf{u}^{d}_{k+1} - \mathbf{u}^{d}_{k} \end{bmatrix}.
\end{aligned} \tag{60}$$

The temporal discretization in this work is performed using the convolution quadrature scheme, which efficiently approximates the Caputo fractional derivative as a weighted sum of all previous solution values. The reaction term, characterized by the parameter λ, enters the system as an additional algebraic term proportional to $u(t)$, without altering the underlying fractional weights. This extended formulation results in a highly flexible and accurate BEM framework for time-fractional diffusion-reaction equations. This approach facilitates a systematic investigation of the influence of λ on the spatio-temporal evolution of the solution, enabling rigorous validation against analytical expansions.

Following established conventions, the resulting approach is referred to as CD-BEM. In this notation, "C" denotes the use of the Caputo fractional derivative, and "D" indicates the presence of a domain integral in the BEM formulation. This notation highlights the essential features of the method and underscores its applicability to a wide class of time-fractional problems.

6 Numerical results and discussion

In this section, we examine the performance of the proposed CD-BEM through representative numerical examples. We first outline the computational procedure in order to clarify the main implementation steps of the method. Subsequently, we present and compare the numerical results with the corresponding analytical solutions to assess the accuracy and applicability of the proposed formulation under different problem settings.

6.1 Implementation outline of the proposed CD-BEM

We organize the numerical implementation within a modular MATLAB framework. The main routine uses the node coordinates, boundary elements, and triangular cell vertices provided in the input file to call dedicated subroutines. These subroutines assemble the matrices, impose the boundary conditions, solve the linear systems, and export the results. The main computational steps are summarized as follows:

1. **Input data:** Read the mesh information (boundary elements and interior triangular cells), physical parameters $(\alpha, \lambda, D_x, D_y)$, time discretization settings $(\Delta t, T)$, and the prescribed initial and boundary conditions.

2. **Initialization:** Define the boundary and interior node sets, initialize the solution vector, and compute the total number of time steps $N_t = T/\Delta t$.

3. **Matrix assembly [19]:** Construct the boundary influence matrices $\mathbf{H}$ and $\mathbf{G}$ together with the domain matrix $\mathbf{M}$, based on the boundary and domain integrals introduced in the previous section. For interior collocation points, the block $\mathbf{H}^{dd}$ includes the identity contribution corresponding to $c(\xi) = 1$.

4. **System setup:** At each time level t_{n+1}, define the unknown vectors $\mathbf{u}^b_{n+1}$, $\mathbf{u}^d_{n+1}$, and $\mathbf{q}^b_{n+1}$, and collect all terms associated with the current time level on the left-hand side.

5. **Time-marching loop:** For $n = 0, 1, \ldots, N_t - 1$:

   (a) Compute the fractional history weights and assemble the right-hand-side vector.

   (b) Impose the prescribed Dirichlet and/or Neumann boundary conditions.

   (c) Solve the resulting linear system for the unknown boundary and interior values.

   (d) Store the computed solution for post-processing.

6. **Output:** Export the numerical results for visualization and comparison.

In the present implementation, we evaluate boundary integrals using linear boundary elements, although the overall structure can be adapted straightforwardly to constant elements if needed. We perform numerical integration by Gaussian quadrature, using two- to ten-point rules according to the required level of accuracy. The implementation targets the fractional-order regime $0 < \alpha < 1$, consistent with the scope of the proposed formulation.

For validation purposes, we compute the analytical solution in MATLAB using the Mittag-Leffler function for both cases with and without the reaction term λ. Since the entire numerical framework, including the CD-BEM solver, is implemented in MATLAB, we evaluate the Mittag-Leffler function using the MATLAB routine originally developed by Garrappa [18]. This routine has also been ported to other languages. For example, the `khinsen/mittag-leffler` repository provides a Python port of the same algorithm. However, the present work adopts the MATLAB version directly. In this way, both the analytical benchmark and the numerical CD-BEM solution are computed within the same MATLAB environment. This choice ensures full consistency between the reference and numerical results. We then compare the corresponding CD-BEM results systematically with these analytical solutions. For the one-dimensional reduction of the problem, we neglect the variation in the y-direction. The analytical solution is then given by Equation (27), which provides the closed-form solution of the fractional diffusion-reaction equation.

6.2 Example 1: Rectangular domain with effectively one-dimensional behavior

The first numerical experiment considers a rectangular region

$$\Omega = \{(x,y) \mid 0 \le x \le L_x,\ 0 \le y \le L_y\}, \tag{61}$$

with $L_x = 2$ and $L_y = 1$. The governing problem is given by Equation (1), with isotropic diffusion coefficients $D_x = D_y = D$. We examine a diffusion-reaction scenario in which the transported quantity moves from the left boundary toward the right boundary. For spatial discretization, we employ the mesh shown in Figure 2, rescaled so that the mesh boundaries coincide with the physical domain boundaries.

Available at: https://github.com/khinsen/mittag-leffler

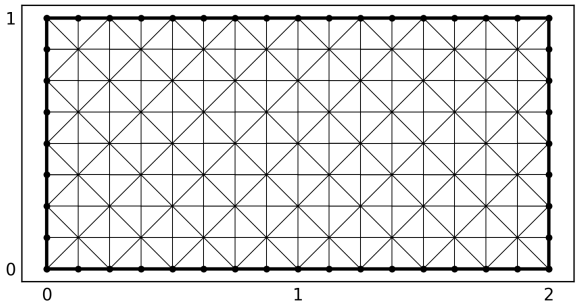

Figure 2: Spatial discretization mesh configuration used in this study, rescaled so that the mesh boundaries coincide with the physical domain boundaries.

The Dirichlet boundary conditions are prescribed on the two vertical sides as:

$$u(0,y,T) = 10, \qquad u(L_x,y,T) = 0, \qquad 0 \le y \le L_y. \tag{62}$$

On the horizontal boundaries $y = 0$ and $y = L_y$, homogeneous Neumann conditions are imposed, implying zero normal diffusive flux. Using Fick's law, the normal flux is written as

$$J(x,y,t) = -D\frac{\partial u}{\partial n}, \tag{63}$$

where D is the isotropic diffusion coefficient and $\frac{\partial u}{\partial n}$ is the normal derivative of the concentration u with respect to the boundary. Thus, the Neumann conditions can be written as

$$J(x,0,T) = 0, \qquad J(x,L_y,T) = 0, \qquad 0 \le x \le L_x. \tag{64}$$

The initial condition prescribes a uniform zero concentration within the domain

$$u(x,y,0) = u_0(x,y) = 0. \tag{65}$$

The computational mesh consists of 52 boundary nodes, 105 interior nodes, 48 boundary elements, and 256 triangular cells. For the initial test, we evaluate the CD-BEM solution using the parameter set $\alpha = 0.5$, $\lambda = 0.001$, $D = 1$, and $T = 2$. Owing to the homogeneous Neumann boundary conditions prescribed along $y = 0$ and $y = L_y$, the physical response remains effectively one-dimensional across this rectangular domain. To assess the accuracy of the numerical scheme, we compare these CD-BEM results against the analytical solution and against a one-dimensional fully implicit L1 finite difference method (L1-FDM). The L1-FDM reference is computed with a spatial step size of $h_x = 0.125$ and $N_t = 400$ time steps.

The results in Table 1 show that the CD-BEM solution remains close to the analytical reference along the line $y = 0.5$. The computed profile is smooth and monotone between the two Dirichlet boundaries, without visible spurious oscillations. The additional comparison with the one-dimensional L1-FDM solution provides independent support for the correctness of the proposed CD-BEM implementation for this benchmark problem.

Table 1: Pointwise comparison of the analytical solution, CD-BEM, and 1D L1-FDM at $T = 2.0$ ($\alpha = 0.5$, $\lambda = 0.001$, $D = 1$, $h_x = 0.125$)

Node	x	y	$u_{\text{Analytical}}$	$u_{\text{CD-BEM}}$	u_{FDM}	$\lvert e\rvert_{\text{BEM}}$	$\lvert e\rvert_{\text{FDM}}$	Rel_{BEM} (%)	Rel_{FDM} (%)
1	0.000	0.500	10.0000000000	10.0000000000	10.0000000000	0.00e+00	0.00e+00	0.0000	0.0000
2	0.125	0.500	9.0796551966	9.0793112631	9.0798769643	3.44e-04	2.22e-04	0.0038	0.0024
3	0.250	0.500	8.2176502584	8.2180926712	8.2180550310	4.42e-04	4.05e-04	0.0054	0.0049
4	0.375	0.500	7.4097742761	7.4108510148	7.4103242573	1.08e-03	5.50e-04	0.0145	0.0074
5	0.500	0.500	6.6518483444	6.6534117307	6.6525071485	1.56e-03	6.59e-04	0.0235	0.0099
6	0.625	0.500	5.9397359068	5.9416513505	5.9404689334	1.92e-03	7.33e-04	0.0322	0.0123
7	0.750	0.500	5.2693501471	5.2714980947	5.2701248939	2.15e-03	7.75e-04	0.0408	0.0147
8	0.875	0.500	4.6366587056	4.6389330753	4.6374450273	2.27e-03	7.86e-04	0.0491	0.0170
9	1.000	0.500	4.0376859891	4.0399919796	4.0384563079	2.31e-03	7.70e-04	0.0571	0.0191
10	1.125	0.500	3.4685133323	3.4707654535	3.4692428085	2.25e-03	7.29e-04	0.0649	0.0210
11	1.250	0.500	2.9252772618	2.9273977648	2.9259439288	2.12e-03	6.67e-04	0.0725	0.0228
12	1.375	0.500	2.4041661020	2.4060838493	2.4047509723	1.92e-03	5.85e-04	0.0798	0.0243
13	1.500	0.500	1.9014151535	1.9030650491	1.9019022998	1.65e-03	4.87e-04	0.0868	0.0256
14	1.625	0.500	1.4133006655	1.4146239822	1.4136772823	1.32e-03	3.77e-04	0.0936	0.0266
15	1.750	0.500	0.9361328171	0.9370790411	0.9363892651	9.46e-04	2.56e-04	0.1011	0.0274
16	1.875	0.500	0.4662479138	0.4667787151	0.4663777507	5.31e-04	1.30e-04	0.1138	0.0278
17	2.000	0.500	0.0000000000	0.0000000000	0.0000000000	0.00e+00	0.00e+00	0.0000	0.0000

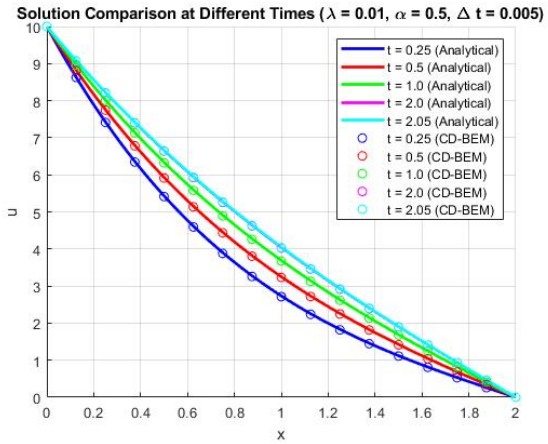

Figure 3: Spatial distribution of $u(x,T)$ for $\alpha = 0.5$, $\lambda = 0.01$, and $\Delta t = 0.005$ at different time levels

Figure 3 compares the analytical and CD-BEM solutions at several time levels for $\alpha = 0.5$. The numerical profiles remain close to the analytical ones throughout the spatial domain, and the solution evolves smoothly as T increases.

Figure 4 presents the spatial profiles corresponding to different values of α at $T = 2.05$. The results show that the fractional order influences both the amplitude and the spatial variation of the solution. In particular, smaller α values lead to steeper decay in the spatial profile, whereas larger values produce a more gradual variation. For all tested cases, the CD-BEM results remain close to the corresponding analytical curves.

Figure 5 shows the temporal evolution of the solution at the interior point $x = 1.0$ for different fractional orders. The results indicate that varying α changes the transient response of the system, consistent with the memory effect of the time-fractional model. Larger α values produce faster growth and higher attained levels, while smaller α values yield a slower and smoother temporal response. Throughout the

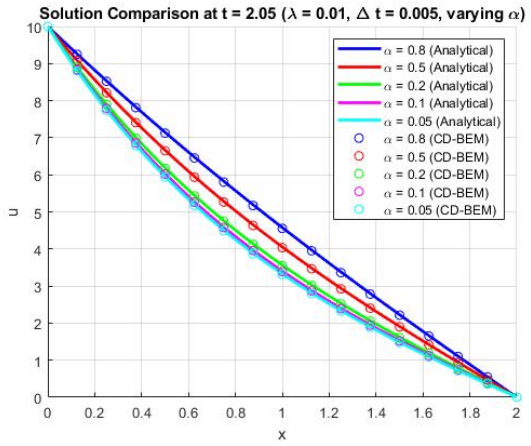

Figure 4: Comparison of $u(x,T)$ for different fractional orders α at $T = 2.05$ ($\lambda = 0.01$, $\Delta t = 0.005$)

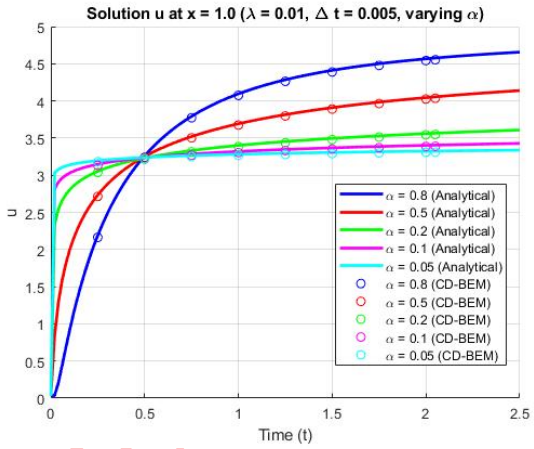

Figure 5: Solution $u(x,T)$ at $x = 1.0$ for various α values ($\lambda = 0.01$, $\Delta t = 0.005$): analytical and CD-BEM results

displayed time interval, the CD-BEM curves remain close to the analytical ones.

6.2.1 Effect of the fractional order on error and solution profiles

The fractional order α plays a decisive role in both the accuracy and convergence behavior of the proposed extended CD-BEM. As shown in Figures 6(a) and 6(b), smaller α values produce smoother temporal evolution, resulting in lower spatial oscillations in the relative error and faster numerical convergence. Specifically, for $\alpha = 0.01$, the relative error remains uniformly small across the domain, whereas for $\alpha = 0.5$, sharper temporal variations and higher localized errors are evident.

The analytical–numerical comparisons in Figures 6(c) and 6(d) further demonstrate that decreasing α not only improves agreement with the exact solution but also reduces discrepancies in regions with steep gradients. As α approaches unity, the increased temporal stiffness amplifies numerical challenges, potentially impairing convergence rates. From a modeling perspective, weakly fractional systems

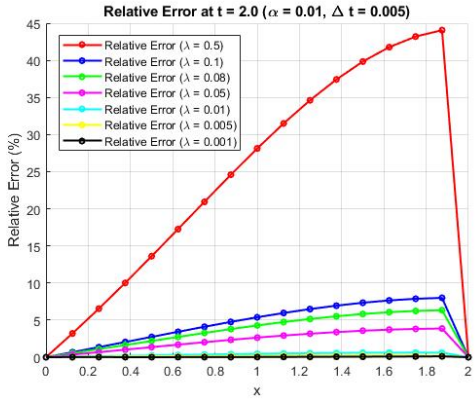

(a) Relative error ($\alpha = 0.01$, $\Delta t = 0.005$).

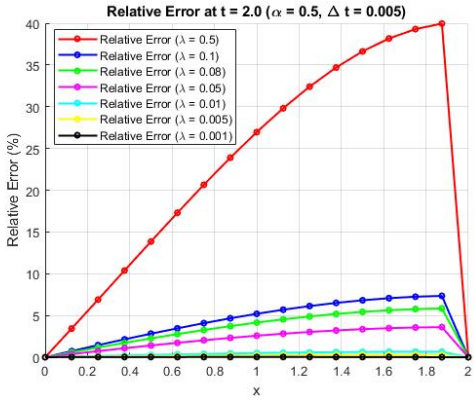

(b) Relative error ($\alpha = 0.5$, $\Delta t = 0.005$).

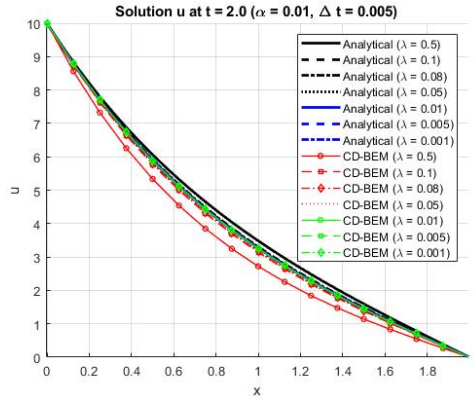

(c) Analytical vs CD-BEM $u(x)$ ($\alpha = 0.01$).

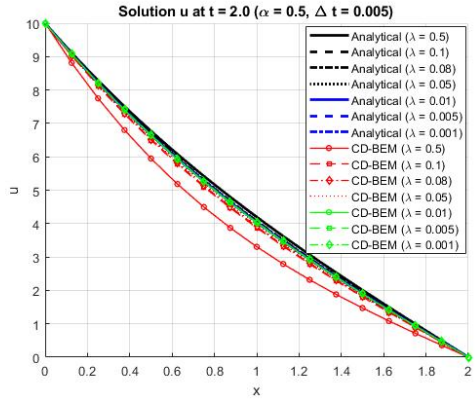

(d) Analytical vs CD-BEM $u(x)$ ($\alpha = 0.5$).

Figure 6: (a)–(b) Relative error (%) along the spatial domain x at $T = 2.0$ for various λ values, shown for two fractional orders α. (c)–(d) Comparison between analytical solutions, shown by lines, and CD-BEM solutions, shown by markers, for $u(x)$ with the same α values. The results show that larger λ values produce higher relative errors and steeper decay, while smaller α yields smoother evolution and lower overall errors.

($\alpha \ll 1$) are particularly advantageous. They effectively capture subdiffusive transport processes while simultaneously benefiting from improved numerical stability and efficiency.

6.2.2 Effect of the reaction coefficient λ and stability analysis

Figure 7 compares the analytical and numerical solutions at $T = 2.0$ for various λ values, with fractional order $\alpha = 0.05$ and $\Delta t = 0.005$. The curves reveal that the reaction coefficient λ has a pronounced influence on both the amplitude and spatial decay rate of the solution. For $\lambda = 0.5$, the solution decays more steeply, reflecting a strong reaction term that accelerates concentration reduction. As λ decreases, the decay slope reduces and the numerical curves approach the analytical ones more closely, indicating higher accuracy. For very small λ (e.g., $\lambda \leq 0.1$), fractional diffusion dominates the dynamics. This yields excellent agreement between the numerical and analytical solutions, with negligible deviation

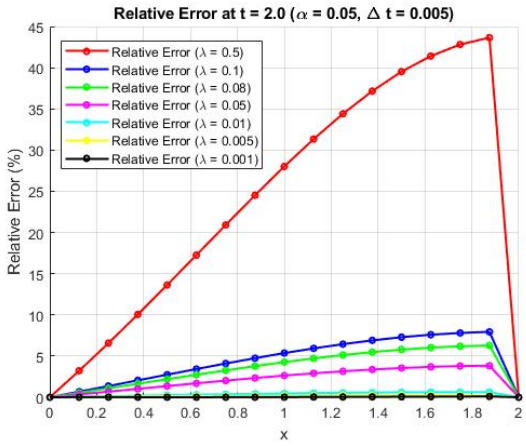

Figure 7: Comparison of analytical and numerical solutions u along the spatial domain x at $T = 2.0$ for $\alpha = 0.05$ and $\Delta t = 0.005$, with various reaction coefficients λ. Stronger reactions (λ large) lead to steeper decay and greater sensitivity to discretization, whereas weaker reactions (λ small) result in diffusion-dominated dynamics and excellent numerical agreement.

Table 2: Relative error (L_∞ norm) at $T = 2.0$ for $\alpha = 0.05$ and $\Delta t = 0.005$

λ	Relative Error
0.5	0.0816
0.1	0.0179
0.08	0.0144
0.05	0.0090
0.01	0.0016
0.005	0.0007
0.001	0.0001

across the domain.

Table 2 quantitatively confirms the visual trends: as λ decreases from 0.5 to 0.001, the L_∞-norm relative error monotonically drops from 8.16×10^{-2} to 1×10^{-4}. This clear inverse relationship highlights the enhanced robustness of the extended BEM formulation for weakly reactive regimes, where the smoothness of the solution facilitates accurate boundary integral representation and stable temporal evolution.

The increase of the numerical error for larger values of the reaction coefficient λ can be explained through a stability consideration of the fractional reaction–diffusion operator. Consider the simplified governing equation

$$D_t^\alpha u = D\nabla^2 u - \lambda u. \tag{66}$$

To analyze the stability behavior, we represent the solution using a spatial Fourier mode

$$u(x,t) = e^{ikx} v(t), \tag{67}$$

which reduces Equation (66) to the fractional ordinary differential equation

$$D_t^\alpha v(t) = -(Dk^2 + \lambda) v(t). \tag{68}$$

Table 3: L_∞ and L_2 relative errors and estimated temporal convergence rates at $T = 2.0$ for $\alpha = 0.5$ and $\lambda = 0.01$

Δt	$E_{\mathrm{rel},\infty}$	$E_{\mathrm{rel},2}$	Rate p_∞	Rate p_2
0.1	1.186606×10^{-3}	1.552482×10^{-3}	—	—
0.05	5.447829×10^{-4}	7.129097×10^{-4}	1.1231	1.1228
0.01	5.855942×10^{-5}	7.665204×10^{-5}	1.3858	1.3856
0.005	— (reference)	—	—	—

The analytical solution of Equation (68) is given in terms of the Mittag–Leffler function

$$v(t) = E_\alpha\left(-(Dk^2 + \lambda)t^\alpha\right), \tag{69}$$

which shows that the effective decay rate of each mode depends on the parameter

$$\mu = Dk^2 + \lambda. \tag{70}$$

As λ increases, the magnitude of μ becomes larger and the system exhibits stronger stiffness. For time-discretized fractional schemes, stability typically requires a constraint of the form

$$\Delta t^\alpha (Dk^2 + \lambda) \lesssim C, \tag{71}$$

where C is a constant depending on the numerical scheme. Therefore, when λ increases while Δt remains fixed, condition (71) becomes more restrictive. As a result, discretization errors may increase. This theoretical observation explains the numerical behavior reported in Table (2). For relatively large reaction coefficients ($\lambda \geq 0.5$), the reaction term dominates the dynamics and increases the stiffness of the system, leading to larger numerical errors. In contrast, when λ is small ($\lambda \leq 0.1$), the problem becomes diffusion-dominated and the extended BEM formulation produces highly accurate numerical results with very small relative errors.

6.2.3 Temporal accuracy and convergence analysis

We examine the temporal accuracy of the proposed CD-BEM formulation for the rectangular test problem with $\alpha = 0.5$, $\lambda = 0.01$, and final time $T = 2.0$. To isolate the temporal error, the spatial discretization is kept fixed while the time step size is successively refined. The relative error is evaluated in both the L_∞ and the L_2 norms as

$$E_{\mathrm{rel},\infty} = \frac{\|u_{\mathrm{num}} - u_{\mathrm{exact}}\|_\infty}{\|u_{\mathrm{exact}}\|_\infty}, \qquad E_{\mathrm{rel},2} = \frac{\|u_{\mathrm{num}} - u_{\mathrm{exact}}\|_2}{\|u_{\mathrm{exact}}\|_2}, \tag{72}$$

where the L_2 norm is evaluated with the discrete ℓ_2-norm over the spatial grid, thereby providing a complementary accuracy measure that accounts for the error over the whole domain rather than at a single worst grid point only. The temporal convergence rate is estimated from two consecutive time steps according to

$$p \approx \frac{\log(E_1/E_2)}{\log(\Delta t_1/\Delta t_2)}, \tag{73}$$

where E_1 and E_2 denote the relative errors corresponding to Δt_1 and Δt_2, respectively.

As shown in Table 3, the relative error decreases systematically with time-step refinement in both the L_∞ and L_2 norms. The two norms yield very close values at each time step, and their estimated convergence rates agree well. These rates range from approximately 1.1 to 1.4, indicating an approximately first-order temporal convergence behavior for the present computations.

We discretize the time-fractional derivative using the L1 scheme. For sufficiently smooth solutions, the L1 approximation of the Caputo derivative has a formal temporal accuracy of $O(\Delta t^{2-\alpha})$. In the present case, this formal order would be $O(\Delta t^{1.5})$ for $\alpha = 0.5$.. However, solutions of time-fractional diffusion-reaction problems commonly possess limited temporal regularity near the initial time. In particular, the solution may exhibit a weak initial singularity at $t = 0$. This singularity prevents the smoothness required to attain the formal $2-\alpha$ order on a uniform temporal mesh.

Consequently, the observed convergence rate of the L1 scheme may decrease toward first order under uniform time discretization. The rates reported in Table 3 are therefore consistent with the expected practical behavior of L1-based temporal discretization for time-fractional diffusion-reaction problems [40, 46, 48]. These results also confirm that the proposed extended CD-BEM formulation remains stable and accurate under temporal refinement.

6.2.4 Computational cost and memory requirements

The direct discretization of the Caputo fractional derivative involves a historical memory effect. As a result, it leads to a convolution structure in which the solution at time t_n depends on all preceding time levels. Consequently, the computational complexity scales as $O(N_t^2)$. To assess the practical feasibility and temporal scaling of our implementation, we measured the CPU execution times on a workstation equipped with an Intel Core i5-10210U CPU (1.60 GHz) and 8 GB of RAM.

To assess the practical feasibility and temporal scaling of our implementation, we measured the CPU execution times on a workstation equipped with an Intel Core i5-10210U CPU (1.60 GHz) and 8 GB of RAM. For the fractional diffusion-reaction case with $\alpha = 0.5$ and $\lambda = 0.01$, the CPU times were recorded for three different time-step sizes while keeping the spatial discretization and other parameters fixed, as summarized in Table 4: 8.63s, 21.09s and 58.98s for $N_t = 200$, 400 and 800, respectively. Taking the case $N_t = 200$ as the reference, the corresponding relative computational costs are 1.0000, 2.4438 and 6.8366, with effective scaling exponents of approximately 1.29 and 1.48 over the two successive refinement intervals (overall exponent 1.39).

These results demonstrate a clear superlinear growth of the computational cost with the number of time steps, consistent with the increasing burden of the history-term evaluation and its tendency toward the expected $O(N_t^2)$ behavior for finer temporal discretizations. The reference integer-order case with $\alpha = 1.0$ required $t_{\mathrm{CPU}}^{\alpha=1.0} = 1.12$ s, whereas the fractional diffusion-reaction case with $\alpha = 0.5$, spatial discretization $h = 0.125$, and time step $\Delta t = 0.005$ resulted in $t_{\mathrm{CPU}}^{\alpha=0.5} = 21.09$ s. The computational cost ratio is defined as

$$\frac{t_{\mathrm{CPU}}^{\alpha=0.5}}{t_{\mathrm{CPU}}^{\alpha=1.0}} = \frac{21.09}{1.12} \approx 18.83. \tag{74}$$

This issue has been widely discussed in the literature on fractional numerical methods, where various acceleration techniques have been proposed. In particular, adaptive time stepping reduces the total number of time levels by taking larger steps when the solution varies slowly and refining locally near sharp transient regions, which can shorten the overall simulation time considerably. Reduced-memory schemes, on the other hand, avoid storing, referencing and evaluating the full temporal history required

Table 4: CPU-time scaling with respect to the number of time steps for $\alpha = 0.5$ and $\lambda = 0.01$ (fixed $h = 0.125$)

N_t	Δt	CPU time (s)	Relative cost
200	0.01	8.63	1.0000
400	0.005	21.09	2.4438
800	0.0025	58.98	6.8366

by the non-local Caputo derivative; for instance, they may retain only a fixed number of previous values or use a compressed approximation of the history term, thereby significantly lowering memory usage and the cost of the history-related convolution sums. Recent developments addressing computational efficiency for fractional models are reported in [11, 46, 47]. Although the present study uses a straightforward implementation of the history term, the CD-BEM framework can in principle be combined with these techniques to further reduce the computational cost in large-scale simulations.

6.3 Example 2: Square domain problem

In this example, the transient transport of a diffusive species in an isotropic medium is examined in the square domain defined by

$$\Omega = \{(x,y) \mid 0 \le x \le L_x, 0 \le y \le L_y\}, \qquad L_x = L_y = 2. \tag{75}$$

The time-fractional diffusion-reaction process is governed by the model described in Equation (1), with isotropic diffusion coefficients $D_x = D_y = 1$. The initial and boundary conditions applied here are identical to those defined in Example 1.

For the spatial discretization, the domain is divided into 64 boundary elements with 68 boundary nodes, together with 225 internal nodes and 512 triangular cells. This discretization mesh is illustrated in Figure 8. The temporal discretization is performed using a uniform time step of $\Delta t = 0.005$, and the fractional order is set to $\alpha = 0.01$. The simulation illustrates the gradual migration of the substance under the combined influence of diffusion and a first-order reaction.

Numerical simulations are performed for four reaction rates $\lambda \in \{0.05, 0.01, 0.005, 0.001\}$. For each case, the numerical CD-BEM solution is compared with the corresponding analytical expression given in Equation (27). Figure 9 presents the spatial concentration profiles at the mid-line $y = 1.0$, illustrating the influence of λ on the solution behavior. The CD-BEM results remain close to the analytical curves across all tested reaction rates, supporting the validity and consistency of the numerical formulation in the fractional-order regime. As expected, decreasing the reaction coefficient λ causes the profiles to gradually approach the pure diffusion limit.

Table 5 compares the numerical values of $u(x,y,t)$ along the line $y = 1.0$ at $T = 2.0$ for $\alpha = 0.01$, $\lambda = 0.01$ and $D = 1$. The CD-BEM results remain close to the analytical solution, with the maximum absolute difference staying below 2×10^{-3} across the domain. Furthermore, the L1-FDM results show close agreement with both the analytical and CD-BEM profiles, verifying the consistency of the numerical implementation.

6.3.1 Spatial convergence and mesh refinement analysis

To examine the spatial accuracy of the proposed CD-BEM formulation for the time-fractional diffusion-reaction equation, a mesh-refinement study is carried out on the square domain $\Omega = [0,L] \times [0,L]$ with

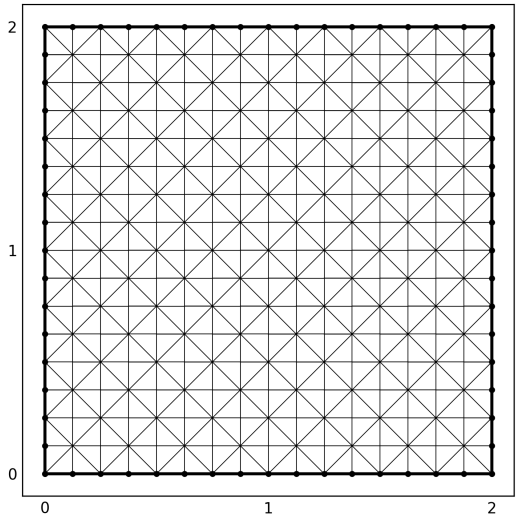

Figure 8: Discretization mesh configuration for the 2×2 square domain, showing the boundary elements and internal triangular cells.

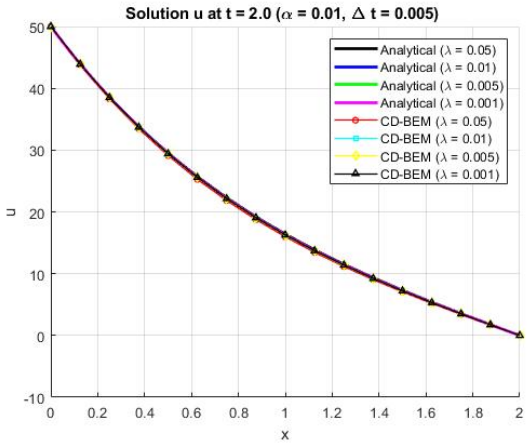

Figure 9: Comparison of CD-BEM numerical results (markers) and analytical solutions (solid lines) at $y = 1.0$ for $\alpha = 0.01$ and four reaction rates: $\lambda = 0.05$, $\lambda = 0.01$, $\lambda = 0.005$, and $\lambda = 0.001$.

$L = 2$. To evaluate the convergence behavior, three progressively refined meshes are employed:

- **Mesh 1:** $N_\Gamma = 32$ boundary elements and $N_\Omega = 128$ interior triangular cells,
- **Mesh 2:** $N_\Gamma = 64$ boundary elements and $N_\Omega = 512$ interior triangular cells,
- **Mesh 3:** $N_\Gamma = 128$ boundary elements and $N_\Omega = 2048$ interior triangular cells.

Let h denote the boundary element length on Γ for a given mesh level. Denoting by E_h the corresponding error (in either the L_∞ or L_2 norm), the observed spatial convergence rate p_s between two

Table 5: Comparison of u values on the line $y = 1$ for $\alpha = 0.01$, $\lambda = 0.01$, $D = 1$, $T = 2.0$

Node	x	y	$u_{\text{Analytical}}$	$u_{\text{FDM 2D}}$	$u_{\text{CD-BEM}}$
1	0.000	1.000	10.00000000	10.0000000000	10.00000000
2	0.125	1.000	8.77948847	8.7586507616	8.77746456
3	0.250	1.000	7.69596434	7.5597499811	7.69338651
4	0.375	1.000	6.73252228	6.4431282391	6.72955138
5	0.500	1.000	5.87413035	5.4337685508	5.87096739
6	0.625	1.000	5.10739547	4.5421913332	5.10427761
7	0.750	1.000	4.42035449	3.7677462939	4.41749198
8	0.875	1.000	3.80228758	3.1025453482	3.79977096
9	1.000	1.000	3.24355099	2.5347972435	3.24135471
10	1.125	1.000	2.73542659	2.0511646271	2.73349894
11	1.250	1.000	2.26998588	1.6382169405	2.26830146
12	1.375	1.000	1.83996629	1.2832047975	1.83852695
13	1.500	1.000	1.43865787	0.9743827434	1.43748060
14	1.625	1.000	1.05979860	0.7010559627	1.05890590
15	1.750	1.000	0.69747674	0.4534699064	0.69689035
16	1.875	1.000	0.34603852	0.2226165872	0.34577550
17	2.000	1.000	0.00000000	0.0000000000	0.00000000

Table 6: Spatial error analysis and observed convergence rates (p_s) for the CD-BEM solution ($\alpha = 0.5, \lambda = 0.001, T = 2.0$) using a fixed time step $\Delta t = 0.005$.

Mesh	h	E_∞	E_{L_2}	p_∞	p_{L_2}
Mesh 1	0.2500	4.827×10^{-3}	3.407×10^{-3}	—	—
Mesh 2	0.1250	3.596×10^{-3}	2.440×10^{-3}	0.425	0.482
Mesh 3	0.0625	2.230×10^{-3}	1.406×10^{-3}	0.689	0.795

successive meshes is computed using the following relation:

$$p_s = \frac{\log(E_{h_1}/E_{h_2})}{\log(h_1/h_2)}. \tag{76}$$

The numerical results presented in Table 6 indicate a steady reduction in both E_∞ and E_{L_2} errors as the spatial mesh is refined under a fixed time step $\Delta t = 0.005$. The calculated convergence rates exhibit an increasing trend from Mesh 1→2 to Mesh 2→3, suggesting that the discretization grid is gradually approaching the asymptotic convergence regime.

The observed rates are sublinear, which may be attributed to the typical limited regularity of fractional-order derivatives near the boundaries and potential geometric singularities arising at the corners of the square domain. Nonetheless, the consistent reduction of the error norms across the refined grids provides supporting evidence for the spatial convergence of the proposed formulation.

6.4 Example 3: Validation on an L-shaped domain

To further assess the applicability of the proposed CD-BEM to non-convex and geometrically more complex domains, we consider the time-fractional diffusion-reaction equation on the L-shaped domain

$$\Omega_{\text{L}} = [0,2] \times [0,0.5] \cup [0,1] \times [0.5,1]. \tag{77}$$

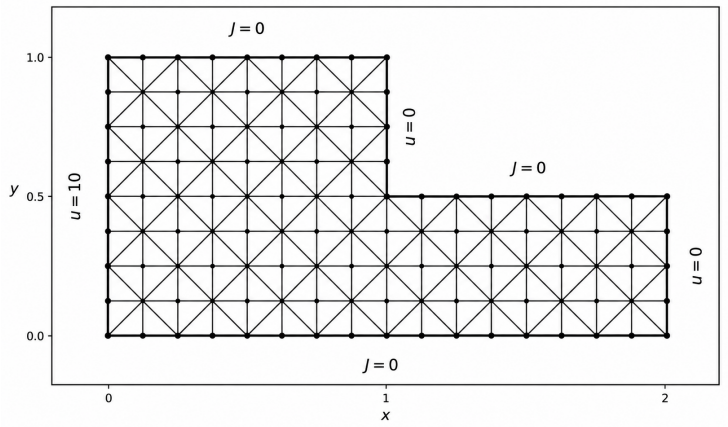

Figure 10: Triangular mesh and boundary-condition configuration for the L-shaped domain used in Example 3.

This geometry contains a re-entrant corner and therefore provides a more demanding test for the numerical method than the rectangular case. The boundary discretization and the auxiliary interior triangulation used for this example are shown in Figure 10.

A mixed boundary condition is prescribed. On the left boundary ($x = 0$), the Dirichlet condition $u = 10$ is imposed. On the right vertical boundary and on the inner vertical boundary of the L-shape, the Dirichlet condition $u = 0$ is prescribed. On the horizontal boundaries, a homogeneous Neumann condition is applied, namely $J = \frac{\partial u}{\partial n} = 0$. The computational parameters are taken as $\alpha = 0.5$, $\lambda = 0.01$, $\Delta t = 0.005$, and $T = 2.0$.

In the CD-BEM formulation, the boundary operators $\mathbf{H}$ and $\mathbf{G}$ are assembled exclusively through boundary elements and boundary integration. However, because of the time-fractional term and the reaction contribution, domain integrals also arise. These integrals are evaluated numerically by triangulating the interior of the L-shaped domain and performing quadrature over the resulting triangular cells. It should be emphasized that this interior triangulation is introduced only for the evaluation of the domain integrals and the associated mass-type contributions. It is not used as a domain discretization of the governing differential operators. The principal unknowns remain associated with the boundary, and the solution procedure retains the boundary-integral character of the proposed CD-BEM.

Since no closed-form analytical solution is available on the present non-convex domain, the performance of the proposed method is assessed through direct comparison with other numerical methods, namely FEM 2D (L1), FDM 2D, and FVM 2D (L1). Table 7 reports the point-wise values of $u(x, 0.25, 2.0)$ along the line $y = 0.25$.

The four numerical solutions display the same overall monotone decay from the imposed value $u = 10$ at the left boundary to $u = 0$ near the right side of the domain. The CD-BEM results remain close to those obtained by the FEM [35] and FDM discretizations over the full observation line, while somewhat larger deviations are observed with respect to the FVM data at several points.

These differences may be attributed to the combined influence of the non-convex geometry, the re-entrant corner, and the distinct discretization mechanisms used by the four methods. In particular, the present example indicates that the proposed CD-BEM remains stable and effective even on geometries with reduced regularity, while preserving its boundary-oriented formulation.

Table 7: Point-wise comparison of the numerical solutions $u(x, 0.25, 2.0)$ obtained by CD-BEM, FEM 2D (L1), FDM 2D, and FVM 2D (L1) on the L-shaped domain with $\alpha = 0.5$, $\lambda = 0.01$, and $\Delta t = 0.005$

Node	x	$u_{\text{CD-BEM}}$	u_{FEM}	u_{FDM}	u_{FVM}
1	0.0000	10.00000000	10.00000000	10.00000000	10.00000000
2	0.1250	8.73331975	8.73350339	8.73572649	8.35012031
3	0.2500	7.52925714	7.51774824	7.53218796	7.32177728
4	0.3750	6.38500627	6.36086633	6.38686265	6.35427076
5	0.5000	5.30121590	5.26268704	5.29885251	5.44958284
6	0.6250	4.28297278	4.22714755	4.27071499	4.61401080
7	0.7500	3.34534712	3.26672757	3.31273627	3.86140959
8	0.8750	2.52609585	2.41285791	2.45333420	3.21758732
9	1.0000	1.89389502	1.73686323	1.76062188	2.71691414
10	1.1250	1.47978836	1.35617672	1.35182064	2.32467460
11	1.2500	1.20321985	1.10204411	1.08224712	1.97333434
12	1.3750	0.97872307	0.89419081	0.87032858	1.64311796
13	1.5000	0.77221549	0.70432115	0.68242215	1.32704107
14	1.6250	0.57381266	0.52290507	0.50556204	1.02155795
15	1.7500	0.38015987	0.34627079	0.33446127	0.72405787
16	1.8750	0.18940166	0.17246044	0.16651078	0.43219225
17	2.0000	0.00000000	0.00000000	0.00000000	0.00000000

Table 8: Point-wise comparison of the absolute errors of FEM, FDM and FVM with respect to CD-BEM for $u(x, 0.25, 2.0)$ on the L-shaped domain with $\alpha = 0.5$, $\lambda = 0.01$, and $\Delta t = 0.005$

Node	x	$\lvert u_{\text{CD-BEM}} - u_{\text{FEM}} \rvert$	$\lvert u_{\text{CD-BEM}} - u_{\text{FDM}} \rvert$	$\lvert u_{\text{CD-BEM}} - u_{\text{FVM}} \rvert$
1	0.0000	0.00000000	0.00000000	0.00000000
2	0.1250	0.00018364	0.00240674	0.38319944
3	0.2500	0.01150890	0.00293082	0.20747986
4	0.3750	0.02413994	0.00185638	0.03073551
5	0.5000	0.03852886	0.00236339	0.14836694
6	0.6250	0.05582523	0.01225779	0.33103802
7	0.7500	0.07861955	0.03261085	0.51606247
8	0.8750	0.11323794	0.07276165	0.69149147
9	1.0000	0.15703179	0.13327314	0.82301912
10	1.1250	0.12361164	0.12796772	0.84488624
11	1.2500	0.10117574	0.12097273	0.77011449
12	1.3750	0.08453226	0.10839449	0.66439489
13	1.5000	0.06789434	0.08979334	0.55482558
14	1.6250	0.05090759	0.06825062	0.44774529
15	1.7500	0.03388908	0.04569860	0.34389800
16	1.8750	0.01694122	0.02289088	0.24279059
17	2.0000	0.00000000	0.00000000	0.00000000

To quantify the agreement between the methods in a more systematic manner, Table 8 reports the point-wise absolute errors of FEM, FDM, and FVM with respect to the CD-BEM solution. The maximum errors are 1.57×10^{-1}, 1.33×10^{-1}, and 8.45×10^{-1}, respectively, and the errors decrease consistently toward the boundary nodes where the solution is prescribed. The close agreement between the

CD-BEM results and those of the well-established FEM and FDM schemes, together with the qualitative consistency observed with respect to FVM, indicates that the proposed method does not introduce spurious deviations on this irregular geometry. Although a closed-form analytical solution is not available for the L-shaped domain, the present comparison demonstrates that the CD-BEM can be regarded as a credible and competitive alternative among the existing numerical approaches.

This example therefore provides supporting evidence that the proposed boundary element implementation for time-fractional diffusion-reaction problems is not restricted to simple rectangular domains and can be extended to more complex geometries such as L-shaped configurations. The numerical experiments performed on rectangular, square and L-shaped domains, together with the theoretical considerations discussed earlier, indicate that the CD-BEM provides a stable and viable framework for this class of problems. Should higher pointwise precision be required, a range of established enhancement strategies documented in the recent literature may be readily incorporated; further improvements in accuracy and extension to more challenging regimes remain subjects for future research [30, 31].

6.5 General discussion and computational aspects

Here we present the theoretical and computational aspects of the proposed CD-BEM scheme derived from the three numerical test cases.

6.5.1 Stability and matrix invertibility considerations

After spatial discretization and temporal discretization of the Caputo fractional derivative, the CD-BEM formulation leads to a linear algebraic system at each time level in the form

$$A\,\mathbf{u}^{n+1} = \mathbf{F}^{n}, \tag{78}$$

where $\mathbf{u}^{n+1}$ denotes the vector of unknown nodal values at time t_{n+1}. The right-hand-side vector $\mathbf{F}^{n}$ includes the contributions of the prescribed boundary data, the solution at previous time levels, and the history terms arising from the Caputo fractional derivative.

The effective system matrix A is constructed from the boundary-element influence matrices and the domain contributions associated with the fractional derivative and reaction terms. Since the precise matrix structure depends on the boundary conditions, the boundary discretization and the treatment of the domain integrals, a general proof of nonsingularity for arbitrary geometries and meshes is not pursued here. Instead, the numerical solvability and conditioning of the discrete systems are examined for the test cases considered in this study.

For the square-domain test case, the estimated condition number of the assembled system matrix A was evaluated by using the MATLAB function `condest`. The results for three boundary-mesh resolutions are listed in Table 9. As the number of boundary elements increases from 32 to 128, the estimated condition number increases from 4.34×10^2 to 1.96×10^3. Such a moderate increase under boundary-mesh refinement is expected for boundary-element influence matrices. Nevertheless, all the systems considered for the square domain were solved without numerical breakdown, indicating satisfactory numerical conditioning for the tested mesh resolutions.

The conditioning of BEM-type influence matrices may deteriorate for highly nonuniform meshes, closely spaced nodes, large element-size variations, and sharp or re-entrant corners, thereby amplifying round-off errors and reducing solver robustness. Therefore, reasonably regular boundary meshes were

used in the present computations. The results in Table 9 provide numerical evidence of reliable solvability for the square-domain meshes considered here, rather than a general proof of invertibility for arbitrary geometries and discretizations.

A conventional von Neumann stability analysis is not directly applicable to the present CD-BEM formulation because the method involves boundary-integral operators, domain-integral contributions, nonuniform boundary discretizations and history terms from the Caputo derivative, rather than a translation-invariant finite-difference stencil. Therefore, the practical numerical robustness of the method is assessed through the solvability of the linear systems, the conditioning results reported above and the mesh- and time-step-refinement studies presented in the numerical examples. Related stability properties of fractional diffusion and diffusion-reaction models are discussed in [29, 45, 49].

Table 9: Estimated condition number of the assembled system matrix A for the square-domain test case under boundary-mesh refinement

Number of boundary elements, N_b	condest(A)
32	4.344575×10^2
64	9.831007×10^2
128	1.959760×10^3

6.5.2 Performance of CD-BEM for anisotropic fractional diffusion-reaction problems

To assess the reliability of the proposed CD-BEM method for solving time-fractional diffusion-reaction equations under anisotropic diffusion, we conducted a numerical experiment on a rectangular domain. The problem was solved with anisotropic diffusion coefficients $D_x = 0.2$ and $D_y = 0.1$, fractional order $\alpha = 0.5$ and reaction coefficient $\lambda = 0.01$. The results of the CD-BEM were compared with the analytical solution as well as the solutions obtained from the FDM and FEM at time $t = 2$ along the line $y = 0.5$.

Figure 11 presents the comparison of the four methods. The CD-BEM solution exhibits reasonable agreement with the analytical solution and successfully captures the overall trend of the problem. However, small deviations are observed, particularly in the middle and right-hand regions of the domain ($x > 0.75$). Among the numerical methods, the FDM provides the closest results to the analytical solution, while the CD-BEM shows larger deviations than the FDM but smaller deviations than the FEM in most parts of the domain.

The observed discrepancies in the CD-BEM results can be mainly attributed to the additional complexity introduced by the anisotropic diffusion coefficients. Anisotropy increases the difficulty in the boundary integral formulation and in the accurate treatment of the fractional time derivative. Furthermore, the approximation of the history term in the fractional operator, differences in spatial discretization schemes, and the fact that the reference analytical solution is derived from a one-dimensional formulation may also contribute to the pointwise differences observed in the two-dimensional implementation.

Despite these deviations, the results indicate that the CD-BEM is capable of reproducing the essential behavior of anisotropic fractional diffusion-reaction problems on rectangular domains.

6.5.3 Convergence analysis and theoretical justification

The convergence behaviour of the proposed CD-BEM formulation is strongly influenced by the limited temporal regularity of solutions to time-fractional diffusion-reaction equations. For the anisotropic

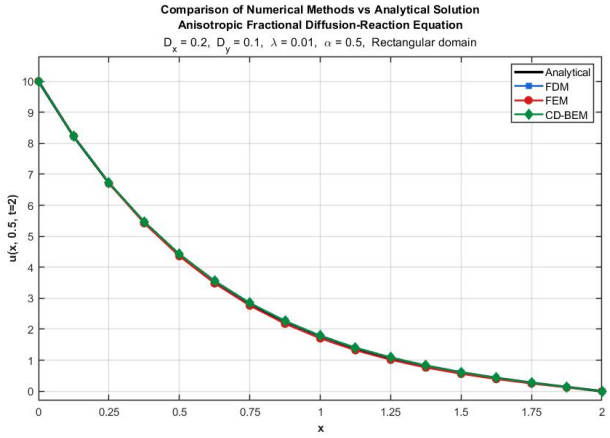

Figure 11: Comparison of the analytical solution with FEM, FDM and CD-BEM for anisotropic diffusion ($D_x = 0.2$, $D_y = 0.1$) in the rectangular domain at $\alpha = 0.5$ and $\lambda = 0.01$

fractional model

$$ {}^{C}D_t^{\alpha} u = D_x \frac{\partial^2 u}{\partial x^2} + D_y \frac{\partial^2 u}{\partial y^2} - \lambda u + f, \tag{79} $$

the solution typically exhibits a weak singularity at the initial time. In particular, the temporal derivatives satisfy

$$ \frac{\partial^k u}{\partial t^k}(t) \sim t^{\alpha-k}, \qquad t \to 0^+. \tag{80} $$

Due to this reduced regularity, numerical methods based on uniform time grids usually achieve only first-order convergence in time, even if higher-order discretizations are employed. In the present CD-BEM, the Caputo derivative is approximated by a convolution quadrature of the form

$$ {}^{C}D_t^{\alpha} u(t_n) = \sum_{k=0}^{n} w_k u(t_{n-k}), \tag{81} $$

which accounts for the entire history of the solution. Consequently, the total error is expected to satisfy

$$ \|u(t_n) - u_n\| \leq C\left(h^{p_s} + \Delta t\right), \tag{82} $$

where h is the spatial discretization parameter, p_s denotes the spatial convergence rate, and the temporal contribution is generally of order $\mathcal{O}(\Delta t)$.

The numerical results obtained in this study show that the observed temporal convergence rate of the CD-BEM is close to first order, which is consistent with the theoretical regularity constraints of fractional diffusion problems. Recent studies on fractional diffusion models, convergence analysis, and advanced discretization techniques can be found in [2, 22, 28, 40, 41, 43, 48, 50].

7 Conclusion

In this study, we developed a Caputo-Domain Boundary Element Method (CD-BEM) for two-dimensional time-fractional diffusion-reaction equations with a linear reaction term. Both isotropic and anisotropic

diffusion cases were considered, and the Caputo derivative was approximated using the L1 time-discretization scheme.

We assessed the method through three numerical examples on square, rectangular, and L-shaped domains. For all examples, the L_∞ and relative errors were evaluated and compared, where applicable, with analytical solutions and with the results of FEM, FDM and FVM. The good agreement obtained in these comparisons confirms the accuracy and consistency of the proposed CD-BEM formulation for different diffusion properties, boundary conditions and geometrical configurations. In particular, the L-shaped example demonstrates its applicability to non-convex domains.

The temporal analysis showed an approximately first-order convergence rate for the L1 scheme on uniform time grids. Moreover, the temporal and spatial stability of the formulation were investigated through the coefficient matrices, their invertibility and their condition numbers. The results showed stable numerical behavior for the considered mesh configurations and parameter values.

Although the direct treatment of the Caputo history term has a quadratic computational cost with respect to the number of time steps, the proposed CD-BEM provides a viable alternative to domain-based methods for the considered fractional diffusion-reaction problems. Future work may focus on fast memory algorithms, non-uniform time meshes, nonlinear reaction terms, variable-order fractional diffusion-reaction models and the extension of the proposed framework to more complex geometries.

Acknowledgment

We are grateful to the Editor and the anonymous reviewers for their constructive comments and suggestions that significantly improved the quality of this manuscript.

Declaration

The authors declare no competing interests.

References

[1] P. Alipour, *The BEM and DRBEM schemes for the numerical solution of the two-dimensional time-fractional diffusion-wave equations*, Nonlinear Studies **30** (2023) 4.

[2] K. Anukiruthika, P. Muthukumar, P. Das, *Semigroup-based theoretical prospects on optimal control of stochastic second-order Gurtin–Pipkin integro-differential equations*, Optimization **75** (2026) 2207–2224.

[3] S. Barmada, S. Dodge, M. Tucci, A. Formisano, P. Di Barba, M. E. Mognaschi, *A novel hybrid boundary element–physics informed neural network method for numerical solutions in electromagnetics*, IEEE Access **12** (2024) 171444–171457.

[4] J.R. Berger, A. Karageorghis, *The method of fundamental solutions for heat conduction in layered materials*, International Journal for Numerical Methods in Engineering **45** (1999) 1681–1694.

[5] R.N. Borkor, A. Sakyi, N.K.-D.O.Opoku, R.E. Eghan, J. Amoah-Mensah, A. Abubakar, K.O. Edusei, P. Amoako-Yirenkyi, *Investigation of fractional compartmental models in pharmacokinetics with application to amiodarone drug diffusion*, Sci. Afr. **28** (2025) e02700.

[6] C.A. Brebbia, J.C.F. Telles, L.C. Wrobel, *Boundary element techniques: theory and applications in engineering*, Springer Science & Business Media, 2012.

[7] J.A.M. Carrer, B. S. Solheid, J. Trevelyan, M. Seaid, *A boundary element method formulation based on the Caputo derivative for the solution of the anomalous diffusion problem*, Engineering Analysis with Boundary Elements **122** (2021) 132–144.

[8] J. A. M. Carrer, C. L. N. Cunha, W. J. Mansur, *The boundary element method applied to the solution of two-dimensional diffusion–advection problems for non-isotropic materials*, Journal of the Brazilian Society of Mechanical Sciences and Engineering **39** (2017) 4533–4545.

[9] J.A.M. Carrer, M. Seaid, J. Trevelyan, B. dos Santos Solheid, *The boundary element method applied to the solution of the anomalous diffusion problem*, Engineering Analysis with Boundary Elements **109** (2019) 129–142.

[10] J.A.M. Carrer, J. Trevelyan, M. Seaid, B.S. Solheid, *A boundary element formulation for PDEs containing fractional derivatives*, in: Proceedings of the 12th UK Conference on Boundary Integral Methods (UKBIM12), 2019, 72.

[11] P. Das, S. Rana, J. Vigo-Aguiar, *Higher order accurate approximations on equidistributed meshes for boundary layer originated mixed type reaction diffusion systems with multiple scale nature*, Appl. Numer. Math. **148** (2020) 79–97.

[12] M. Dehghan, M. Safarpoor, *The dual reciprocity boundary elements method for the linear and nonlinear two-dimensional time-fractional partial differential equations*, Mathematical Methods in the Applied Sciences **39** (2016) 3979–3995.

[13] P.W. Eloe, J.T. Neugebauer, *Green's functions for a fractional boundary value problem with three terms*, Foundations **2** (2022) 885–897.

[14] M.A. Fahmy, M. Toujani, *A New Fractional Boundary Element Model for the 3D Thermal Stress Wave Propagation Problems in Anisotropic Materials*, Mathematical and Computational Applications **30** (2025) 6.

[15] M.A. Fahmy, *Boundary element modeling and simulation algorithm for fractional bio-thermomechanical problems of anisotropic soft tissues*, in: Recent Developments in the Solution of Nonlinear Differential Equations, IntechOpen, 2021, ch. 5.

[16] M.A. Fahmy, A. Almutlg, *Boundary Element Method Solution of a Fractional Bioheat Equation for Memory-Driven Heat Transfer in Biological Tissues*, Fractal and Fractional **9** (2025) 565.

[17] M.A. Fahmy, M. Toujani, *Fractional boundary element solution for nonlinear nonlocal thermoelastic problems of anisotropic fibrous polymer nanomaterials*, Computation **12** (2024) 117.

[18] R. Garrappa, *Numerical evaluation of two and three parameter Mittag-Leffler functions*, SIAM Journal on Numerical Analysis **53** (2015) 1350–1369.

[19] H. Ghassemi, M. Bakhtiari, *Boundary Element Method*, Amirkabir University of Technology Press, Tehran, 2016 (in Persian).

[20] A. Ghezal, A.A. Al Ghafli, H. J. Al Salman, *Anomalous Drug Transport in Biological Tissues: A Caputo Fractional Approach with Non-Classical Boundary Modeling*, Fractal and Fractional **9** (2025) 508.

[21] R. Gorenflo, F. Mainardi, *Fractional calculus: integral and differential equations of fractional order*, in: A. Carpinteri, F. Mainardi (Eds.), Fractals and Fractional Calculus in Continuum Mechanics, Springer, 1997, pp. 223–276.

[22] L. Govindarao, K.S. Al-Ghafri, J. Mohapatra, T. A. Nhan, *Stable and Convergent High-Order Numerical Schemes for Parabolic Integro-Differential Equations with Small Coefficients*, Symmetry **17** (2025) 1475.

[23] B.I. Henry, T.A.M. Langlands, S. L. Wearne, *Anomalous diffusion with linear reaction dynamics: From continuous time random walks to fractional reaction-diffusion equations*, Physical Review E–Statistical, Nonlinear, and Soft Matter Physics **74** (2006) 031116.

[24] V.R. Hosseini, F. Yousefi, W.-N. Zou, *The numerical solution of high dimensional variable-order time-fractional diffusion equation via the singular boundary method*, Journal of Advanced Research **32** (2021) 73–84.

[25] J. Hu, T. Liu, M. Klöhn, et al., *Nucleotide analogue bemnifosbuvir inhibits hepatitis E virus replication in preclinical models*, Gut (2026).

[26] M. Karkulik, J.M. Melenk, A. Rieder, *Stable decompositions of hp-BEM spaces and an optimal Schwarz preconditioner for the hypersingular integral operator in 3D*, ESAIM: Mathematical Modelling and Numerical Analysis **54** (2020) 145–180.

[27] J.T. Katsikadelis, *The BEM for numerical solution of partial fractional differential equations*, Computers & Mathematics with Applications **62** (2011) 891–901.

[28] S. Kumar, P. Das, et al., *Analysis of an efficient parameter uniform domain decomposition approach for singularly perturbed Gierer–Meinhardt type nonlinear coupled systems of parabolic problems*, International Journal of Numerical Analysis and Modeling **22** (2025) 459–482.

[29] S. Kumar, I. R, P. Das, *Impact of mixed boundary conditions and nonsmooth data on layer-originated nonpremixed combustion problems: Higher-order convergence analysis*, Studies in Applied Mathematics **153** (2024) e12763.

[30] S. Kumar, P. Das, K. Kumar, *Adaptive mesh based efficient approximations for Darcy scale precipitation–dissolution models in porous media*, International Journal for Numerical Methods in Fluids **96** (2024) 1415–1444.

[31] S. Kumar, S. Kumar, P. Das, *Second-order a priori and a posteriori error estimations for integral boundary value problems of nonlinear singularly perturbed parameterized form*, Numerical Algorithms **99** (2025) 1365–1392.

[32] Ch. Lage, Ch. Schwab, *On the implementation of a fully discrete multiscale Galerkin BEM*, WIT Trans. Model. Simul. **18** (1997) 635–644.

[33] J. Ma, D. Liu, J. Wu, X. Li, *Normalized Fourier-induced PINN method for solving the wave propagation equation in a non-unitized domain over an extended time range*, arXiv:2503.05716 (2025).

[34] E. Majchrzak, B. Mochnacki, *Analysis of thermal processes occuring in tissue with a tumor region using BEM*, Journal of Theoretical and Applied Mechanics **40** (2002) 101–112.

[35] X. Meng, J.L. Gracia, M. Stynes, *Local analysis of an L1/finite element method for a time-fractional singularly perturbed reaction-diffusion problem*, Numer. Algor. (2025) 1–36.

[36] R. Metzler, J. Klafter, *The random walk's guide to anomalous diffusion: a fractional dynamics approach*, Physics Reports **339** (2000) 1–77.

[37] K.S. Miller, B. Ross, *An Introduction to the Fractional Calculus and Fractional Differential Equations*, John Wiley & Sons, 1993.

[38] J.D. Murray, *Mathematical biology: I. An introduction*, Springer Science & Business Media, 2007.

[39] J.D. Murray, *Mathematical biology II: Spatial models and biomedical applications*, Springer, New York, 2003.

[40] A. Patawari, P. Das, *From traditional to computationally efficient scientific computing algorithms in option pricing: Current progresses with future directions*, Arch. Comput. Methods Eng. **33** (2026) 1699–1738.

[41] A. Patawari, S. Kumar, P. Das, *A modified iterative PINN algorithm for strongly coupled system of boundary layer originated convection diffusion reaction problems in MHD flows with analysis*, Netw. Heterog. Media **20** (2025) 1026–1060.

[42] I. Podlubny, *Fractional differential equations: an introduction to fractional derivatives, fractional differential equations, to methods of their solution and some of their applications*, Elsevier, 1998.

[43] P.A. Prince, L. Govindarao, S. Elango, *Richardson extrapolation for singularly perturbed Fredholm integro-differential equations*, Int. J. Math. Eng. Manag. Sci. **10** (2025) 094.

[44] V. Raghavan, G. Lavidas, A. V. Metrikine, *Comparing Open-Source BEM solvers for analysing wave energy converters*, Journal of Physics: Conference Series **2647** (2024) 072002.

[45] Y.A. Sabawi, S. Santra, P. Das, N. A. Mohammad, H^1 *stability and convergence analysis of the L1/L1-2 Legendre spectral method for non-local weakly singular integro-PDEs*, Calcolo **62** (2025) 1–46.

[46] S. Saini, P. Das, S. Kumar, *Computational cost reduction for coupled system of multiple scale reaction-diffusion problems with mixed type boundary conditions having boundary layers*, Rev. R. Acad. Cienc. Exactas Fis. Nat. Ser. A Mat. **117** (2023) 66.

[47] S. Saini, P. Das, S. Kumar, *Parameter uniform higher order numerical treatment for singularly perturbed Robin type parabolic reaction-diffusion multiple scale problems with large delay in time*, Appl. Numer. Math. **196** (2024) 1–21.

[48] S. Santra, P. Das, P. Jorgensen, *A unified multifaceted space-time wavelet framework and its singularity analysis for weakly singular non-local partial integro-differential equations in high dimensions*, Acta Applicandae Mathematicae **200** (2025) 1–42.

[49] S. Santra, J. Mohapatra, P. Das, D. Choudhuri, *Higher order approximations for fractional order integro-parabolic partial differential equations on an adaptive mesh with error analysis*, Computers & Mathematics with Applications **150** (2023) 87–101.

[50] V. Saw, P. Das, H.M. Srivastava, *Investigations of a class of Liouville–Caputo fractional order Pennes bioheat flow partial differential equations through orthogonal polynomials on collocation points*, Bull. Sci. Math. **201** (2025) 103637.

[51] R.K. Saxena, A.M. Mathai, H. J. Haubold, *Fractional reaction-diffusion equations*, Astrophys. Space Sci. **305** (2006) 289–296.

[52] K. Seki, M. Wojcik, M. Tachiya, *Fractional reaction-diffusion equation*, J. Chem. Phys. **119** (2003) 2165–2170.

[53] A.V. Shapovalov, S.A. Siniukov, *Fractal dynamics of solution moments for the KPP–Fisher equation*, Russ. Phys. J. **67** (2024) 1827–1837.

[54] H. Sun, Y. Zhang, D. Baleanu, W. Chen, Y. Chen, *A new collection of real world applications of fractional calculus in science and engineering*, Commun. Nonlinear Sci. Numer. Simul. **64** (2018) 213–231.

[55] S. Thakur, H. Mitra, A.M. Ardekani, *Physics-informed neural network-based inverse framework for time-fractional differential equations for rheology*, Biology **14** (2025) 779.

[56] A.M. Turing, *The chemical basis of morphogenesis*, Bull. Math. Biol. **52** (1990) 153–197.

[57] M. Vellappandi, S. Lee, *Role of fractional derivatives in pharmacokinetic/pharmacodynamic anesthesia model using BIS data*, Comput. Biol. Med. **187** (2025) 109783.

[58] A.R. Ynineb, E. Yumuk, D. Copot, et al., *Modeling drug retention as memory effects in obese patients using fractional and augmented models*, Scientific Reports **15** (2025) 26234.

[59] M.A. Zaitri, H. Zitane, D.F.M. Torres, *Pharmacokinetic/pharmacodynamic anesthesia model incorporating psi-Caputo fractional derivatives*, Comput. Biol. Med. **167** (2023) 107679.

[60] M. Zakaria and A. Moujahid, *On Galerkin spectral element method for solving Riesz fractional diffusion equation based on Legendre polynomials*, J. Math. Model. 13(2) (2025) 281–301.

[61] H. Zhang, X. Jiang, F. Zeng, G.E. Karniadakis, *A stabilized semi-implicit Fourier spectral method for nonlinear space-fractional reaction-diffusion equations*, Journal of Computational Physics **405** (2020) 109141.